Historical dynamics of terrestrial carbon during 1901-2016 as simulated by the CLM-Microbe model

Liyuan He[1], Jorge L. Mazza Rodrigues[2], Melanie A. Mayes[3], Chun-Ta Lai[1], David A. Lipson[1], Xiaofeng Xu*[1]

1. Biology Department, San Diego State University, San Diego, CA, 92182, USA
2. Department of Land, Air and Water Resources, University of California - Davis, Davis, CA 95616, USA
3. Environmental Sciences Division and Climate Change Science Institute, Oak Ridge National Laboratory, Oak Ridge, Tennessee, 37831, USA

Correspondence: Xiaofeng Xu (xxu@sdsu.edu)

Abstract. Soil microbes play a crucial role in carbon (C) cycle; however, terrestrial C cycle during historical period with soil microbial role considered is still unknown. We applied a microbial-explicit Earth system model – the Community Land Model (CLM)-Microbe – to investigate the dynamics of C in vegetation, litter, soil, and microbes during 1901-2016. The CLM-Microbe model was able to reproduce the variations of gross (GPP) and net (NPP) primary productivity, heterotrophic (HR), and soil (SR) respiration, microbial (MBC) biomass C in fungi (FBC) and bacteria (BBC) in the top 30 cm and 1 m, dissolved (DOC) and soil organic C (SOC) in the top 30 cm and 1 m during 1901-2016. During the study period, simulated C variables increased by approximately 30 PgC yr^{-1} for GPP, 13 PgC yr^{-1} for NPP, 12 PgC yr^{-1} for HR, 25 PgC yr^{-1} for SR, 1.0 PgC for FBC and 0.4 PgC for BBC in 0-30 cm, 1.2 PgC for FBC, 0.7 PgC for BBC, 2.4 PgC for DOC, 34 PgC for SOC, and 4 PgC for litter C in 0-1 m, and 37 PgC for vegetation C. Increases in C fluxes and pools were widely found, particularly at high latitudes and in equatorial regions, but we also observed their decreases in some grids. Overall, we observed significant correlations between the area-weighted averages of GPP, NPP, and vegetation C and those of MAT and MAP. Similarly, the area-weighted averages of HR, SR, and FBC, BBC, DOC, SOC, and litter C in the top 1 m were significantly correlated with that of ST and SM in the top 1 m. These results suggested that vegetation productivity was primarily controlled by warming and precipitation, while microbial and soil C were jointly governed by vegetation C input and soil temperature and moisture. Our simulations revealed the spatial and temporal patterns of terrestrial C cycling responses to environmental change with explicit representation of microbial mechanisms, laying the foundation for an improved understanding of soil microbial roles in the global terrestrial C cycle.

1 Introduction

The atmospheric concentration of carbon dioxide (CO_2) has been drastically increased due to fossil fuel combustion and land-use change since the Industrial Revolution (IPCC, 2001, 2013; Lal, 2004, 2008). The radiative forcing caused by the CO_2 enrichment in the atmosphere has led to an increase in the global surface temperature, known as climate warming (IPCC, 2001). The increases of atmospheric CO_2 and induced warming climate have induced cascading environmental issues and impacted the carbon (C) cycle (Matson et al., 2002; Meeran et al., 2021; Soong et al., 2021).

Previous studies have assessed the effects of climate change on the global C cycle using Earth system models (ESMs) (Bonan et al., 2019; Todd-Brown et al., 2013). For example, Bonan et al. (2019) compared vegetation productivity, heterotrophic respiration, and vegetation and soil C stocks in the Community Land Model (CLM) forced by two climate reconstructions (CRUNCEPv7 and GSWP3v1) (Dirmeyer et al., 2006; Viovy, 2018). These models, however, were developed with an implicit representation of microbial processes, assuming that respired CO_2 is proportional to the soil C stock and leaving unspecified the role of microbes in decomposition processes. Given the critical role that soil microorganisms play in soil biogeochemical processes and their sensitivity to environmental changes, explicit incorporation of soil microbial respiration and activities in decomposition processes into ESMs is considered to be essential to improve the prediction of global C cycling (He et al., 2021a; Wang et al., 2015; Wang et al., 2017; Wieder et al., 2013). Recently, researchers have applied microbial-explicit models in investigating responses of global C cycle to environmental change. For example, Wieder et al. (2015) examined the responses of soil, vegetation, and litter C pools to environmental change using the MIMICS model. Wang et al. (2017) also investigated the impacts of environmental change on enzymes, soil, and microbial biomass C pools using the TRIPLEX-MICROBE model. However, the validation of microbial biomass at coarse scales (e.g., global or biome levels) may introduce uncertainties in the model, particularly in soil microbial biomass and microbe-mediated processes, which can further affect the predicted soil C cycle in those models.

Fungi and bacteria, the two major soil microbial groups, respond differently to environmental change, and differences in their physiological traits concerning biogeochemical processes have been incorporated into the CLM-Microbe model (He et al., 2021a; He et al., 2021b). For example, fungi decrease more than bacteria under N fertilization (Demoling et al., 2008), whereas fungi are less sensitive than bacteria to water stress (Manzoni et al., 2012). Therefore, validating fungal and bacterial biomass in the CLM-Microbe model at the grid level instead of coarse comparisons at global or biome levels may reduce uncertainties in model predictions. Changes in fungal and bacterial abundance can primarily affect terrestrial C cycling considering their distinct roles in biogeochemical processes such as the decomposition of organic materials (Bailey et al., 2002; Boer et al., 2005; Hršelová et al., 1999). Predicting changes in the spatial pattern of fungi and bacteria at the global scale and identifying their controls are essential for understanding the impacts of environmental changes on the global terrestrial C cycle.

To fill the gaps, we investigated the effects of environmental change on the global C cycle using the CLM-Microbe model. The CLM-Microbe model, mechanistically representing microbial mechanisms of soil C cycling and differentiating the physiology of two major microbial functional groups (i.e., fungi and bacteria), provides a feasible way to investigate the effects of environmental change on soil C cycling mediated by soil microbes and reveal the roles of different kingdoms of microbes on C cycling (He et al., 2021a). In this study, we aimed to investigate the effects of environmental change on the global C cycle from 1901 to 2016. We first evaluated the performance of the CLM-Microbe model in reproducing soil, vegetation, and microbial C variables, including gross (GPP) and net (NPP) primary productivity, fungal (FBC) and bacterial (BBC) biomass C in the top 30 cm and 1 m, heterotrophic (HR) and soil (SR) respiration, and dissolved (DOC) and soil (SOC) organic C in the top 30 cm and 1 m. Then, we investigated the effects of environmental change on the temporal trend of variables related to soil, vegetation, microbial, and litter C, including GPP, NPP, HR, SR, FBC, and BBC in the top 30 cm, FBC, BBC, DOC, SOC, and litter C (LitC) in the top 1 m, and vegetation C (VegC) from 1901 to 2016. Finally, we investigated spatial patterns and external environmental controls of changes in those fluxes and pools from 1901 to 2016.

2 Materials and methods

2.1 Model representation of fungal and bacterial biomass

The CLM-Microbe model was built on the model framework developed by Xu et al. (2014) and the default CLM4.5 (hereafter CLM4.5) (Koven et al., 2013). It has been coupled with a microbial functional group–based methane module (Wang et al., 2022; Wang et al., 2019; Xu et al., 2015) and applied to quantify the fungal and bacterial biomass dynamics in natural ecosystems (He et al., 2021a). Taken together, the CLM-Microbe model has unique modules of microbe-mediated decomposition cascades and microbial functional group-mediated methane cycle, with other biogeochemical, thermal, and hydrological processes the same as the CLM4.5. The CLM4.5 classifies litter into three pools, i.e., litter 1 (labile), litter 2 (cellulose), and litter 3 (lignin), and soil organic matter (SOM), materials left during later stages of organic C decay, into four pools, i.e., SOM 1, SOM 2, SOM 3, and SOM 4 (low-high recalcitrance). The three litter pools and four SOM pools differ in base decomposition rate (τ), with turnover times of litter pools ranging from 20 hours to 71 days and turnover times of SOM pools ranging from 14 days to 27 years (Figure. S1). Coarse woody debris (CWD) is fragmented, decomposed, and gradually transferred into litter pools and further from litter to SOM pools (Thornton et al. 2007; Koven et al. 2013). In addition to eight C pools (three litter, four SOM, and CWD pools) in the CLM4.5, we introduced dissolved organic matter (DOM) and fungal and bacterial biomass pools in the CLM-Microbe model. The code for the CLM-Microbe model has been archived at GitHub since 2015. The model version used in this study was checked out

on May 1, 2021, and was archived at Xu et al. (2022).

In the CLM-Microbe model, fungal and bacterial biomasses are the balance between C assimilation (C flow from the decomposition of SOM, DOM, and litter) and C loss through microbial lysis and microbial respiration. Specifically, fungi and bacteria receive C through the transitions from litter, DOM, and SOM pools; fungi and bacteria lose C through the transitions from fungal and bacterial biomass pools to DOM and SOM pools and the atmosphere. The conceptual diagram of the CLM-Microbe model and major parameters are in Figure. S1 and Table S1, respectively.

The decomposition rates of SOM, DOM, and litter are controlled by both their potential decomposition rates and environmental conditions. The decomposition processes in the CLM-Microbe model are defined following the below equations,

$$D_C = k \times r_{depth} \times r_{tsoil} \times r_{water} \times r_{O_2} \quad \text{equation (1)}$$

$$r_{depth} = \exp\left(-\frac{z}{z_\tau}\right) \quad \text{equation (2)}$$

$$r_{tsoil} = Q_{10}^{\frac{T_{soil,j}-T_{ref}}{10}} \quad \text{equation (3)}$$

$$r_{water} = \begin{cases} 0 & for\ \varphi_j < \varphi_{min} \\ \frac{log\left(\varphi_{min}/\varphi_j\right)}{log\left(\varphi_{min}/\varphi_{max}\right)} & for\ \varphi_{min} \le \varphi_j \le \varphi_{max} \\ 1 & for\ \varphi_j > \varphi_{max} \end{cases} \quad \text{equation (4)}$$

$$r_{O_2} = f_r \times (1 - f_{inun}) \times max\left(O_{2_{unsat}}, O_{2_{min}}\right) + f_{inun} \times max\left(O_{2_{sat}}, O_{2_{min}}\right) \quad \text{equation (5)}$$

where D_C is the rate of substrate (e.g., SOM, DOM, and litter) breakdown (in per day); k is the potential decomposition rate (in per day); r_{O_2} represents the environmental modifier determined by soil oxygen concentration (unitless); r_{depth} is the environmental modifier determined by soil depth (unitless); r_{water} is environmental modifier determined by soil moisture (unitless); r_{tsoil} means the environmental modifier determined by soil temperature (unitless); z means soil depth (in m); z_τ is the e-folding depth for decomposition (in m); $T_{soil,j}$ is soil temperature at layer j (in Kelvin); T_{ref} is the reference temperature for decomposition (in Kelvin), which is set as a Kelvin temperature equals to 25°C; Q_{10} indicates the temperature dependence of decomposition, it is the ratio of the rate at a specific temperature to that at 10°C lower (unitless); Ψ_j is the soil water potential in layer j (in MPa); Ψ_{min} is a lower limit for soil water potential control on decomposition rate (set to -10 MPa), r_{water} will be set as 0 if Ψ_j is lower than Ψ_{min} (in MPa); Ψ_{max} is the upper limit for soil water potential control on decomposition, which equals to the saturated soil matric potential, r_{water} will be set as 1 if Ψ_j is higher than Ψ_{max}; $w_{soil,j}$ means soil water content in layer j (in MPa); f_r is the rooting fraction by soil depth (unitless); f_{inun} means the fraction of inundated area (unitless); $O_{2_{unsat}}$ represents the oxygen available to that demanded by roots and aerobic microbes in unsaturated area (unitless); $O_{2_{min}}$ denotes the ratio between minimum anaerobic decomposition rate and

potential aerobic decomposition rate in soil (set to 0.2) (unitless); $O_{2_{sat}}$ represents the oxygen available to that demanded by roots and aerobic microbes in saturated area (unitless); r_{O_2} will be set as 1 in oxic conditions, while it will be estimated as the weighted average of oxygen stress in saturated and unsaturated areas in anoxic conditions (unitless).

Carbon use efficiency (CUE) of soil microbes for assimilating three litter pools in the CLM-Microbe model are determined following the equation in Sinsabaugh et al. (2013). In addition, CUE is reported to vary with temperature, showing a coefficient of -0.012 with increasing temperature (Devêvre and Horwáth 2000). Therefore, we assumed that CUE decreased compared with the ambient thermal regime of microbes' habitats following the equation as below (Xu et al. 2014),

$$\mathrm{CUE} = \left(\mathrm{CUE}_{\max} - CUE_T \times \left(T - T_{CUEref}\right)\right) \times \left({M_{\mathrm{C:N}}}/{S_{\mathrm{C:N}}}\right)^{0.6} \quad \text{equation (6)}$$

where *CUE* is carbon use efficiency, which is defined as the growth-to-assimilation ratio for soil microbes; CUE_{max} is the maximum value of C use efficiency; CUE_T is the coefficient indicating the dependence of C use efficiency on temperature; T_{CUEref} is the reference temperature of C use efficiency, which is defined as 15°C in the CLM-Microbe model; $M_{C:N}$ means the C:N ratio of soil microbial biomass, which is defined as 8 in the CLM-Microbe model; $S_{C:N}$ represents C:N ratio of the substrate (e.g., litter).

The C flow from litter and SOM pools to soil microbes will be partitioned by fungal and bacterial biomass pools based on the C:N ratio of fungal and bacterial biomass. The fraction factor quantifying bacteria C gain from litter and SOM is calculated based on the weighted average of assimilation efficiency of fungi and bacteria following the equation as below,

$$fb = \frac{\left({B_{\mathrm{C:N}}}/{S_{\mathrm{C:N}}}\right)^{0.6}}{\left({F_{\mathrm{C:N}}}/{S_{\mathrm{C:N}}}\right)^{0.6} + \left({F_{\mathrm{C:N}}}/{S_{\mathrm{C:N}}}\right)^{0.6}} \quad \text{equation (7)}$$

$$ff = 1 - fb$$

where *fb* is the fraction of C flowing into bacteria; *ff* is the fraction of C flowing into fungi; $B_{C:N}$ means the C:N ratio of BBC; $F_{C:N}$ means the C:N ratio of FBC; $S_{C:N}$ represents C:N ratio of substrates (e.g., litter and SOM).

Fungi and bacteria have different turnover times; hence, different lysis rate constants were adopted for fungi and bacteria in the CLM-Microbe model (He et al., 2021a). In addition, bacterial and fungal growth is highly sensitive to environmental conditions, such as soil moisture and temperature. As a result, in the CLM-Microbe model, fungal and bacterial biomass lysis is represented as the interactive effects of their lysis rate constants and environmental factors, i.e., r_{O_2}, r_{water}, r_{tsoil}, and r_{depth}, as described above. Microbial respiration is widely affected by multiple abiotic and biotic factors, such as substrate concentration and availability, soil moisture, and soil temperature (Gomez-Casanovas et al., 2012; Zhang et al., 2013). Therefore, in the CLM-Microbe model, fungal

and bacterial respirations are represented as the interactive effects of substrates (i.e., DOM, SOM, and litter), environmental factors (i.e., r_{O_2}, r_{water}, and r_{tsoil}), and fraction factors quantifying C being respired by fungi and bacteria in transitions (Table S1). Fungal and bacterial biomass turnover and microbial respiration are defined following below equations,

$$L = k_M \times r_{depth} \times r_{tsoil} \times r_{water} \times r_{O_2} \quad \text{equation (8)}$$

$$R = D_C \times f_{resp} \quad \text{equation (9)}$$

where L denotes the lysis rate of fungal and bacterial biomass (in per day); k_M is the potential turnover rate of fungal (k_{fungi}) or bacterial ($k_{bacteria}$) biomass (in per day); R represents the microbial respiration rate (in per day); f_{resp} is the fraction factor defining the proportion of C released as respiration during decomposition (unitless).

The CLM-Microbe model treats N in the exactly same framework as CLM4.5, it fully coupled C and nitrogen (N) dynamics in land components. Net N mineralization, the inorganic N supply in the soil for plant uptake, is heavily dependent on microbial immobilization of N. Microbial immobilization of N during decomposition steps depends on C:N ratio of organic materials for decomposition, the C:N ratio of fungal and bacterial biomass, and microbial CUE. The sum of potential immobilization over all immobilization in the biogeochemistry cascade is used to estimate microbial demand of mineral N. For each time step, such microbial mineral N demand is in competition with the total plant N demand of all plant functional types (PFTs) on a soil column. Once this competition has been resolved, actual immobilization is calculated as a proportion of potential immobilization, with the same proportion applied to all immobilization steps (Thornton et al., 2007). Remaining plant N demand summed over all PFTs indicates the demand-based competition between plants and microbes for soil mineral N resource on a column. Unmet plant N demand results in C supply surplus, which is translated back to the direct downregulation of photosynthetic rate and the reduction of GPP. Unmet plant N demand can also indirectly induce the reduced allocation to new growth on light capture in plants. Such consequences imply impacts of N limitation exerted by microbial competition for mineral N on plants, which can in turn affect soil microbial community through subsequent inputs of organic matter of various qualities.

2.2 Representation of fungal- and bacterial-mediated processes by column

In the CLM-Microbe model, land surface heterogeneity was represented using a hierarchical data structure, which is adapted from CLM4.5. Each land grid cell can contain multiple land units (e.g., glacier, lake, wetland, urban, vegetated land, and cropland) and each land unit can be further divided into multiple soil/snow columns. On the vegetated land units, multiple (up to 16) PFTs distinct in physiology and structure from different climate zones (e.g., needleleaf-evergreen-tree-boreal vs. needleleaf-deciduous-tree-boreal, broadleaf-evergreen-tree-tropical vs. broadleaf-deciduous-tree-tropical, and c3-arctic-grass vs. c3-non-arctic-grass) can

occupy space on the column. All vegetation fluxes and state variables were defined at the PFT level, while soil fluxes and state variables were defined at the column level.

In the CLM4.5 and early versions of the CLM-Microbe model (before January 2021), parameters related to soil processes, such as decomposition, were assumed to be homogenous across data structure levels. Our previous work suggested the differences in microbial processes among biomes (He et al., 2021a), the implicitly accounted sub-grid microbial processes may introduce uncertainties in the estimation of soil and microbial fluxes and state variables. Since soil flux and state variables in the CLM-Microbe model are defined at the column level, we represented the heterogeneity of microbe-mediated processes by column. Each PFT shares similar physical, phylogenetic and phenological characteristics, we thus assigned the parameter set of microbial properties by PFT. Furthermore, we determined the microbial properties of each column by the relative weight of PFTs occupied on the column, with the parameter set of the most dominant PFT adopted to represent the microbial and soil processes (e.g., fungal and bacterial biomass turnover rate, DOM degradation rate, and fungal and bacterial C assimilation proportion from SOM, litter, and DOM) on the column.

2.3 Model forcing data

The forcing data for the CLM-Microbe model include meteorological variables such as air temperature, relative humidity, incoming solar radiation, longwave radiation, precipitation rate, surface pressure, and surface winds. In this study, we used the CRUNCEP dataset to force the CLM-Microbe model, which has been widely used to force the CLM. The CRUNCEP dataset is a combination of two existing datasets, i.e., the Climate Research Center timeseries (CRU TS) dataset of 0.5° × 0.5° at a monthly scale and the National Centers for Environmental Prediction (NCEP) reanalysis dataset of 2.5° × 2.5° at 6-hourly scale. In the CRUNCEP dataset, the diurnal and daily variation of variables such as the air temperature, precipitation, humidity, solar radiation, surface pressure, downward longwave radiation, and wind speed were derived from NCEP dataset, while their monthly means are bias corrected by the CRU TS dataset. In this study, the CRUNCEP dataset version 7, with a spatial resolution of 0.5° × 0.5°, spanning from 1901 to 2016, was used to drive the model simulation (Viovy, 2018).

In addition to the meteorological data, we forced the CLM-Microbe model using time-varying CO_2 concentration, N deposition, and aerosol concentration to estimate the C cycle change in the last century, provided by National Center for Atmospheric Research (NCAR) for forcing the CLM offline simulations. Atmospheric N deposition during 1849-2006 with a spatial resolution of 1.25° longitude × 0.9° latitude was applied for all simulations. The CO_2 concentrations remained fixed at 1850 levels (284.7 ppm) for accelerated decomposition and final runs and followed by transient historical (1849-2006) changes in the transient run. The aerosol

concentration in accelerated decomposition and final runs for offline simulation was prescribed at 1850 level, while aerosol concentration with a spatial resolution of 1.25° longitude × 0.9° latitude during 1765-2005 was used in the transient simulation. The transient land use and land cover change during the historical period is based on the dataset of the UNH Transient Land Use and Land Cover Change Dataset Version 1 (LUHa.v1), covering the period of 1850-2005, which was produced by University of New Hampshire research group (Louise Chini, George Hurtt, Steve Frolking; https://luh.umd.edu/readme_LUHa_v1.shtml).

2.4 Model implementation

The model implementation was carried out in three stages, with the spatial resolution of the simulations being 2.5° longitude × 1.9° latitude. First, we ran the accelerated decomposition spin-up to allow the system to reach its steady state (Koven et al., 2013; Thornton & Rosenbloom, 2005). We set the model simulations to 1200 years for the accelerated decomposition phase to reach the steady state (Figure S2). Then, we ran a final spin-up of 100 years to ensure the system was ready for transient simulations during 1850-2016. For the model years of 1850-1900 in transient simulations, we cycled atmospheric forcing during 1901-1910 of the CRUNCEP dataset version 7 to force the model. Then, we used the atmospheric data during 1901-2016 of the CRUNCEP dataset version 7 to drive the simulation between 1901 and 2016. The CLM-Microbe model was initially parameterized for fungal and bacterial mediated processes using time-series data of fungal and bacterial biomass carbon, HR, and SR by biome, and the initial setting for microbial parameters by PFT was adopted from He et al. (2021a) and He et al. (2021b). Specifically, we assigned same microbial parameters for PFTs found in a biome as their initial setting, since our previous parametrization for microbial processes were biome specific. For example, broadleaf-evergreen-tree-tropical and broadleaf-deciduous-tree-tropical, belonging to the biome of Tropical/Subtropical forests, parameter set for Tropical/Subtropical forests biome were applied for PFTs of broadleaf-evergreen-tree-tropical and broadleaf-deciduous-tree-tropical in initial simulations.

2.5 Validation data

Several datasets were employed in this study for model validation. To produce realistic soil conditions in the CLM-Microbe model at the grid level, we used datasets of SOC in the top 1 m soil profile from the Harmonized World Soil Database (HWSD) at 0.05-degree spatial resolution archived at Oak Ridge National Laboratory (Wieder, 2014) and SOC in the top 30 cm from the Global Soil Organic C Map (GSOCmap) version 1.5 at a spatial resolution of 1 km provided by Food and Agriculture Organization of the United Nations (FAO, 2018) to validate the SOC in the top 1 m and 30 cm of the CLM-Microbe model, respectively. To guarantee the reasonability of vegetation productivity, GPP and NPP of MODIS gridded datasets with a spatial resolution of 30 seconds during 2000-2015 were used to compare with the simulated GPP and NPP, respectively (Zhao et al., 2005). To reproduce the soil

C emission flux, SR and HR from Global Gridded 1-km Annual Soil Respiration Database (SRDB) version 3 available at Oak Ridge National Laboratory were used to validate SR and HR, respectively (Warner et al., 2019). For FBC and BBC in the top 30 cm, the dataset of FBC and BBC with a resolution of 0.5 degrees obtained from He et al. (2020) was used to validate FBC and BBC in the top 30 cm in the CLM-Microbe model, respectively. Microbial biomass C (MBC), the sum of FBC and BBC, in the top 1 m of the CLM-Microbe model outputs were compared with Xu et al. (2013) for accuracy. The DOC in 0-30 cm and 0-1 m with a resolution of 0.5 degrees derived from Guo et al. (2020) were used to compare with that in the top 30 cm and 1 m, respectively, from the CLM-Microbe output for validation. More details about the datasets used for validation can be found in Table S4. Ten-year (2000-2009) averages of simulated soil, vegetation, and microbial variables from the CLM-Microbe output were calculated to compare with those from observed datasets previously described.

To assess the efficacy of the CLM-Microbe model, the available soil and vegetation variables from the CLM4.5, including GPP, NPP, HR, SR, and SOC in the top 30 cm and 1 m, were adopted for comparison. The simulation results during 1850-2014 was forced using GSWP3v1 (Dirmeyer et al., 2006), with environmental changing factors including N deposition and rising CO_2 considered in the historical simulation. The GPP, NPP, HR, SR, and SOC in the top 30 cm and 1 m were provided by Climate Data Gateway at National Center for Atmospheric Research (NCAR). The GPP, NPP, HR, SR, and SOC in the top 30 cm and 1 m were from CLM land-only release. All variables were at a resolution of 0.9° latitude × 1.25° longitude. The temporal resolutions were different among variables; GPP, NPP, SR, and HR are of a monthly output, whereas SOC in 0-30 cm and 0-1 m are of yearly simulations. Ten-year (2000-2009) averages of the CLM4.5-simulated GPP, NPP, HR, SR, and SOC (0-30 cm and 0-1 m) were calculated to represent the long-term soil and vegetation status and for comparison with observed variables.

Since observational datasets and model simulations are of different resolutions and 0.5 degree is the most widely used, we used the function of linint2 in NCAR Command Language to interpolate those datasets and model outputs from their original resolutions to 0.5 degrees. To make the maps comparable, we used the *nibble* and *extracted by mask* functions provided by ArcGIS version 10.2 (ESRI, Redlands, California, USA) to make all maps consistent in geographical boundary and missing values.

2.6 Model parameterization

Although most processes in the CLM-Microbe model were adapted from the CLM4.5, the modification of microbe-mediated decomposition cascades and microbial functional group-mediated methane cycle may reduce the applicability of default parameters in the CLM4.5, Therefore, we performed the parameterization against observational data of FBC and BBC in He et al., (2021a) and HR and SR in He et al., (2021b), with at least two sites in each biome (one for calibration and the rest for validation). Before

the parameterization, we guaranteed the reasonable soil and vegetation conditions by comparing the simulated NPP and SOC with observational data. To calibrate DOC simulated in the model, we collected reported observational data from previous publications. When selecting the data, we ensured that observational DOC in the top 30 cm and 1 m were from natural biomes and each biome included at least two sites (Table S2-3). We calibrated the DOC in the top 30 cm and 1 m by plotting the simulated DOC in the top 30 cm and 1 m against observational data, and we found good performance of the CLM-Microbe in reproducing the observed DOC in both top 30 cm (R^2=0.6, P<0.0001) and 1 m (R^2=0.6, P<0.0001) (Figure S3).

Despite the good performance the CLM-Microbe model in calibration phase using observational data at the site scale, minor adjustments of parameters were necessary to capture variations at the global scale. We optimized the model parameters related to plant, soil, and microbial processes based on SOC in the top 30 cm from GSOCmap and that in the top 1 m from HWSD dataset, vegetation GPP and NPP from MODIS, SR, and HR from SRDB, FBC and BBC (0-30 cm) in He et al. (2020), MBC in Xu et al. (2013), and DOC (0-30 cm and 0-1 m) in Guo et al. (2020). We primarily focused on parameters related to plant photosynthesis (e.g., *flnr*), e-folding factor for decomposition (e.g., *decomp_depth_efolding*) to match the reported GPP, NPP, and SOC in the top 0-30 cm and 1 m. To calibrate the model to fit the observed FBC, BBC, and DOC, we adjusted parameters related to soil microbial (*k_fungi* and *k_bacteria*) and DOC (*k_dom*) turnover, microbial C assimilation efficiency (*m_rf_s1m*, *m_rf_s2m*, *m_rf_s3m*, and *m_rf_s4m*), the proportion of C being released as respiration (*m_batm_f* and *m_fatm_f*), plant C allocation (froot_leaf), and the N concentration of plant tissues (*leafcn* and *frootcn*) to optimize the model simulations of FBC, BBC, MBC, DOC, SR, and HR.

2.7 Model evaluation

To evaluate the model performance in capturing the spatial variation in soil and vegetation variables, we compared GPP, NPP, HR, SR, FBC and BBC in the top 30 cm, MBC (0-1 m), and DOC and SOC (0-30 cm and 0-1 m) reported by the observational datasets and simulated averages of these variables during 2000-2009. Due to the non-normality of those variables, Spearman's rank correlation was used to evaluate the overall model performance for those variables. The Spearman's rank correlation coefficient (r_s), measuring the strength and direction of association between two ranked variables, was calculated following the equation as below,

$$r_s = \frac{cov(R(x),R(y))}{\sigma_{R(x)}\sigma_{R(y)}} \quad \text{equation (10)}$$

where r_s is the Spearman's rank correlation coefficient; R(x) means the rankings of variable x; R(y) indicates the rankings of variable y; cov(R(x),R(y)) is the covariance of R(x) and R(y); $\sigma_{(R(x)}$ and $\sigma_{R(y)}$ are the standard deviations of the rankings of variable x and y, respectively.

2.8 Statistical analysis

Due to the non-normality of simulated and observed GPP, NPP, HR, SR, FBC and BBC in the top 30 cm, MBC (0-1 m), and DOC and SOC (0-30 cm and 0-1 m), we examined the agreement between variables simulated by the CLM-Microbe model or CLM4.5 during 2000-2009 and corresponding observed values at the grid level using Spearman's rank-order correlation. Such analyses were conducted using the function of *cor.test* with a method of *spearman* in "stats" package in R (R Core Team, 2013). The differences in soil, vegetation, litter, and microbial variables between decadal averages of 1901-1910 and 2007-2016 were examined using an independent t-test, conducted with the function of *t.test* in "stats" package in R (R Core Team, 2013) by continents and with the function of *ttest* in NCAR Command Language (https://www.ncl.ucar.edu) by grid.

To identify external environmental controls of soil, vegetation, litter, and microbial variables, we examined the correlations between vegetation productivity and mean annual temperature (MAT) and precipitation (MAP) and correlations of soil temperature (ST) and moisture (SM) with soil, litter, and microbial variables with respect to their area-weighted averages at the grid level from 1901 to 2016. Considering the consistent but stronger environmental influence on soil and microbial variables in the top 30 cm than in the top 1 m, only correlations between external environmental factors and soil and microbial variables in the top 1 m were assessed whether an association exists. The correlations between external environmental factors (e.g., MAP, MAT, SM, and ST) and annual averages of GPP, NPP, HR, SR, VegC, and FBC, BBC, DOC, SOC, and LitC in the top 1 m at the global level during 1901-2016 were estimated using the Pearson's correlation. These statistical analyses above were performed and relevant figures (Figs. 1-7, 10, and 14) were plotted using "graphics" (R Core Team, 2013) and "ggcorrplot" (Kassambara & Kassambara, 2019) packages in R.

To estimate the changing rate of GPP, NPP, HR, SR, FBC and BBC in the top 30 cm, FBC, BBC, DOC, LitC, and SOC in the top 1 m, and VegC during 1901-2016, we conducted linear regression models for these variables with time at the grid level, with the changing rate indicated by the slope of the regression model. In addition, correlations between environmental factors (e.g., MAT, MAP, ST, and SM) and vegetation, soil, litter, and microbial variables including GPP, NPP, HR, SR, VegC, and FBC, BBC, DOC, SOC, and LitC in the top 1 m at the grid level were estimated using Pearson's correlation. Such statistical analyses were performed using NCAR Command Language (https://www.ncl.ucar.edu). Relevant figures (Figs. 8-9, 11-13, and 15-16) were produced using Matlab version 2021b (The MathWorks, Inc.).

3.1 Model validation and comparison with the CLM4.5

The CLM-Microbe produced comparable results with most observed data and performed comparable to or slightly better than the CLM4.5 with respect to the global C budget (Table 1), latitudinal trend (Figures 1 & 2), and individual grid (Figures 3 & 4). The CLM-Microbe model and the CLM4.5 overestimated the GPP by 15.7% and 7.3%, respectively (Table 1). However, NPP simulated by the CLM-Microbe model and the CLM4.5 was overestimated by 1.3% and underestimated by 8.1%, respectively. Similarly, SR was overestimated in both the CLM-Microbe model (15.6%) and the CLM4.5 (4.0%). HR in the CLM-Microbe model and the CLM4.5 was overestimated by 1.7% and underestimated by 4.4%, respectively. Both the CLM-Microbe model and the CLM4.5 underestimated SOC (0-30 cm), by 8.5% and 22.4%, respectively, while SOC (0-1 m) in the CLM-Microbe model and the CLM4.5 was overestimated by 32.4% and underestimated by 21.4%, respectively. The FBC, BBC, MBC, and DOC, only available in the CLM-Microbe model, were better predicted in the top 30 cm than 1 m. The simulated FBC, BBC, and DOC in the top 30 cm were underestimated by 3.3% and overestimated by 26.7% and 24.9%, respectively, while MBC and DOC in the top 1 m were overestimated by 69.5% and 75.0%, respectively.

The CLM-Microbe model can reasonably reproduce the latitudinal trends of vegetation, soil, and microbial variables, with the model performance varied among variables and along soil depth (Figure 1). The latitudinal trends of both GPP and NPP in the CLM-Microbe model agreed with observed data with a slight overestimation at northern latitudes and in equatorial regions, but NPP was slightly underestimated in the southern hemisphere (Figures 1a & 1b). Both HR and SR simulated by the CLM-Microbe model agreed well with observed data in the Southern Hemisphere but were overestimated in equatorial regions and at mid-high latitudes and underestimated at low latitudes in the Northern Hemisphere (Figures 1c & 1d). Similar latitudinal trends of HR and SR were also observed in the CLM4.5 simulation (Figures 2c & 2d). Soil C pools showed similar latitudinal patterns across soil depths (Figures 1e-1k). Specifically, DOC (0-30 cm and 0-1 m) was overestimated in equatorial regions but underestimated in northern temperate regions (Figures 1e-1f). Meanwhile, the CLM-Microbe model produced an overestimation of SOC (0-30 cm and 0-1 m) in equatorial and northern high-latitude regions, but underestimation in northern mid-latitude regions (Figures 1g & 1h). As opposed to the CLM-Microbe model, the CLM4.5 consistently underestimated SOC (0-30 cm and 0-1 m) along latitudes, except for SOC (0-1 m) at latitudes of >60° N. Similarly, both FBC and BBC in the top 30 cm were overestimated in equatorial regions and at northern high latitudes but underestimated in northern mid-latitude regions (Figures 1i & 1j). Overall, FBC (0-30 cm) at southern latitudes was well predicted by the CLM-Microbe model, but BBC (0-30 cm) in that region was underestimated, while MBC (0-1 m) was overestimated across latitudinal gradients (Figure 1k).

At the grid scale, the simulated values of vegetation, soil, and microbial variables with the CLM-Microbe model were significantly consistent with observed (P<0.05; Figure 3). The CLM4.5 also indicated significant consistency between simulated and observed vegetation and soil variables (P<0.05; Figure 4). Overall, both the CLM-Microbe model and CLM4.5 performed better at simulating GPP and NPP than simulating soil and/or microbial variables. The simulated GPP (r_s=0.91) and NPP (r_s=0.86) with the CLM-Microbe model were significantly and positively related to their observed values (Figures 3a & 3b). The GPP (r_s=0.88) and NPP (r_s=0.82) in the CLM4.5 were also significantly and positively associated with observed values (Figures 4a & 4b). The SR tended to be better predicted than HR in both the CLM-Microbe model (r_s=0.70 for SR vs. r_s=0.68 for HR) and the CLM4.5 (r_s=0.68 for SR vs. r_s=0.64 for HR) (Figures 3c & 3d, Figures 4c & 4d). The DOC in 0-1 m (r_s=0.36) was slightly better reproduced than in 0-30 cm (r_s=0.34) in the CLM-Microbe model (Figures 3e & 3f), while both the CLM-Microbe model (r_s=0.68 for 0-30 cm vs. r_s=0.63 for 0-1 m) and CLM4.5 (r_s=0.63 for 0-30 cm vs. r_s=0.59 for 0-1 m) performed better at simulating SOC in the top 30 cm than in the top 1 m (Figures 3g & 3h, Figures 4e & 4f). Similarly, the CLM-Microbe model performed better in simulating FBC and BBC in the top 30 cm than MBC in the top 1 m (r_s=0.43) (Figures 3i-3k). In addition, BBC (r_s=0.53) was better reproduced than FBC (r_s=0.46) in the top 30 cm.

3.2 Carbon fluxes and pools associated with vegetation, litter, microbes, and soil

The GPP, NPP, HR, and SR displayed increasing trends from 1901 to 2016 (Figure 5), with different magnitudes among variables. By 2016, GPP (30 PgC yr^{-1}) increased about twice more than NPP (13 PgC yr^{-1}). Similarly, the increase of SR (25 PgC yr^{-1}) was about twice that of HR (12 PgC yr^{-1}) from 1901. Their increasing rates showed variations with time. We observed a relatively modest increase of GPP, NPP, HR, and SR during 1901-1980, whereas their increase were more rapid from 1981 to 2016.

Microbial, vegetation, litter, and soil C pools increased from 1901 to 2016 despite the year-to-year variability (Figure 6). The VegC, FBC and BBC in the top 30 cm, and FBC, BBC, DOC, SOC, and LitC in the top 1 m increased by about 37, 1.0, 0.4, 1.2, 0.7, 2.4, 34, and 4 PgC, respectively, from 1901 to 2016. However, the temporal trends of those variables varied during 1901-2016. The VegC and LitC and SOC in the top 1 m showed a steady increase during 1901-2016 (Figures 6f & 6h), while FBC (0-30 cm and 0-1 m) decreased from 1901 to 1940 and increased after 1940 (Figures 6a & 6b). The BBC (0-30 cm and 0-1 m) exhibited little change during 1901-1940 but increased rapidly during 1941-2016 (Figures 6c & 6d). The DOC (0-1 m) slightly decreased from 1901 to 1920 but increased after 1920 (Figure 6e).

During 1901-2016, the decadal average of soil C was the largest C pool in the soil-vegetation-litter system, about 15 times of the sum of vegetation and litter C (Table 2). Soil, litter, and vegetation C significantly increased from 1901-1911 to 2007-2016

(P<0.05). However, the absolute increase in those C pools were different, with soil (37.0 PgC) and vegetation (37.1 PgC) increased to a larger extent than litter (5.1 PgC). Although soil and vegetation increased to a similar extent, vegetation (19.2%) showed a larger relative increase than soil (0.8%) due to its smaller pool size. Despite the smallest absolute increase, litter (8.0%) increased more than soil with respect to relative values.

3.3 Spatial pattern of vegetation and soil carbon fluxes

Compared with 1901-1910, GPP, NPP, HR, and SR increased across latitudinal gradients in 2007-2016 (Figure 7). However, the magnitude of the increase differed among latitudinal gradients. Specifically, increases in GPP, NPP, HR, and SR were larger and more prominent at northern latitudes and equatorial regions than at southern latitudes. Across the globe, GPP, NPP, HR, and SR showed similar spatial patterns (Figure 8), and increases in most grids across the globe were statistically significant (P<0.05; Figures 8c, 8f, 8i, and 8l). Correspondingly, we observed positive relative change in most areas from 1901-1910 to 2007-2016 (Figures 8c, 8f, 8i, and 8l). However, we also observed decreases in GPP, NPP, HR, and SR in the grids of South Asia. The GPP, NPP, HR, and SR displayed similar spatial patterns of changing rates (Figures 9). We widely observed significant and positive changing rates of GPP, NPP, HR, and SR from 1901 to 2016 (P<0.05). However, we also found significant negative changing rates of GPP, NPP, HR, and SR in grids of South Asia (P<0.05).

3.4 Spatial pattern of vegetation, litter, microbial, and soil carbon stocks

Similar to C fluxes, C pools in vegetation, soil, microbes, and litter increased across latitudinal gradients from 1901-1910 to 2007-2016 (Figure 10). Overall, FBC and BBC in the top 30 cm, FBC, BBC, DOC, SOC, and LitC in the top 1 m, and VegC showed a small but to different extents of increase across latitudinal gradients. Specifically, the increases were more prominent at northern high latitudes and equatorial regions than at other latitudes.

At the global scale, FBC and BBC in the top 30 cm and 1 m showed similar spatial patterns and widely increased from 1901-1910 to 2007-2016 (Figures 11a & 11b, 11d & 11e, 11g & 11h, and 11j & 11k). Correspondingly, we observed positive relative changes in FBC and BBC in the top 30 cm and 1 m in those regions from 1901-1910 to 2007-2016 (Figures 11c, 11f, 11i, and 11l). Similarly, DOC (0-1 m) showed increases from 1901-1910 to 2007-2016 (Figures 12a & 12b), and the relative changes in DOC (0-1 m) were mostly positive (Figure 12c). We also widely observed increases in SOC (0-1 m) by 2007-2016 relative to 1901-1910 (Figures 12d & 12e), which reached the significance level of 0.05 (Figure 12f). The relative increases were widely positive, while grids of South Asia displayed decreases in SOC (0-1 m) (Figure 12f). The VegC and LitC (0-1 m) exhibited similar spatial patterns and widely

increased across the globe (Figures 12g-12l). The relative change in both VegC and LitC (0-1 m) were mostly positive across the globe, but the magnitudes were different. The relative change in VegC was to a larger extent than in LitC (0-1 m). Despite the widely increase, both VegC and LitC (0-1 m) decreased in South Asia. The FBC and BBC in the top 30 cm, DOC, SOC, and LitC of top1 m, and VegC showed similar spatial patterns of changing rates (Figures 13a-13h). Consistent with the spatial patterns of absolute and relative changes, increasing temporal trends of such variables were widely observed across the globe. However, we also observed decreases of those variables in South Asia (Figures 11-13). In addition, we observed decreases of FBC and BBC in the top 30 cm and FBC, BBC DOC, and SOC in the top 1 m in grids of central North America (Figure 11, Figures 12a-12f, and Figures 13a-13f).

3.5 External environmental controls on C cycling

The area-weighted average of GPP, NPP, and VegC were significantly correlated with those of MAT and MAP (P<0.05; Figure 14a). However, the correlations with MAT are stronger than with MAP. At the grid level, MAP and MAT had widely significant correlations with GPP, NPP, and VegC. The spatial patterns of those correlations were similar among GPP, NPP, and VegC, but different between MAT and MAP (Figure 15). The MAT mostly showed significant positive correlations with GPP, NPP, and VegC (P<0.05; Figures 15a, 15c, and 15e). But we also found significant negative correlations of MAT with GPP, NPP, and VegC in southeast North America, South Asia, southern Africa, and central and northern Australia/Oceania (P<0.05). Despite the similar spatial patterns among GPP, NPP, and VegC in correlations with MAT and MAP, there were differences in the strengths and signs of their correlations. For example, both GPP and VegC had significant positive correlations with MAT in northeast South America (P<0.05), while correlations between NPP and MAT were weak negative in such regions. Both GPP and NPP showed significant positive correlations with MAT in central Africa (P<0.05), while the correlation between VegC and MAT was weak in that area (P>0.05). Significant positive correlations of GPP, NPP, and VegC with MAP were also widely found (P<0.05; Figures 15b, 15d, and 15f). However, we also found weak negative correlations in the northern and east edge of Asia and central Africa. In addition, although correlations of MAP with GPP, NPP, and VegC were similar in spatial patterns, correlations with GPP and NPP tended to be stronger than with VegC.

The area-weighted average of HR, SR, and FBC, BBC, DOC, SOC, and LitC in the top 1 m were significantly correlated with that of ST and SM in the top 1 m (P<0.05; Figure 14b). However, the strengths of correlations depended on both environmental controls (ST and SM in the top 1 m) and variables (HR, SR, and FBC, BBC, DOC, SOC, and LitC in the top 1 m). For example, correlations of HR and SR with ST and SM in the top 1 m were of the same magnitude, while the FBC, BBC, DOC, SOC, and LitC were more strongly correlated with ST than with SM in the top 1 m.

In contrast, soil, litter, and microbial variables were more widely and positively correlated with ST than with SM in the top 1 m (Figure 16). Correlations of ST (0-1 m) with HR and SR were similar in spatial pattern. We widely observed significant positive correlations of HR and SR with ST (0-1 m) (P<0.05; Figures 16a & 16c). While negative correlations of HR and SR with ST (0-1 m) were found in South Asia, southeast North America, central North America, central Africa, and central and northern Australia/Oceania. The FBC, BBC, DOC, and SOC in the top 1 m displayed similar spatial patterns (Figures 16e, 16g, 16i, and 16k). We found significant and positive correlations of FBC, BBC, DOC, and SOC with ST in the top 1 m in most grids across the globe (P<0.05). However, we also found some girds with negative correlations in central North America, Europe, Asia, South America, Africa, and Australia/Oceania. In contrast, correlations between LitC and ST in the top 1 m were equally found to be positive and negative (Figure 16m). Significant positive correlations were observed in central Europe and Asia, northeast South America, central and east coast of Africa, and southern and central Australia/Oceania; while significant negative correlations were distributed in northeast Asia (P<0.05).

Correlations of HR, SR, and FBC, BBC, DOC, and SOC with SM in the top 1 m were similar in spatial patterns, with significant and positive correlations widely observed (P<0.05; Figures 16b, 16d, 16f, 16h, 16j, and 16l). But we also observed negative correlations at middle and low latitudes in North America, Europe, and Asia, east coast of South America and Africa, and southern Australia/Oceania. In contrast, correlations between LitC and SM in the top 1 m were mostly negative and significant (P<0.05; Figure 16n). In addition, some grids with significant and positive correlation coefficients were scattered throughout central Africa, southwest Asia, and central and northern Australia/Oceania (P<0.05).

4 Discussion

4.1 Comparison with previous studies

The latitudinal trends and grid-level distribution of GPP, NPP, HR, SR, FBC and BBC in the top 30 cm, and FBC, BBC, DOC, and SOC in the top 1 m were well-reproduced in the CLM-Microbe model (Figures 1 & 3). The CLM-Microbe model performed better than or comparable to the CLM4.5 in simulating the spatial distribution of vegetation, soil, and microbial variables (Figures 2 & 4). In line with our results, multiple models captured the spatial variation of GPP, NPP, HR, and SR (Delire et al., 2020; Kim et al., 2019; Wiltshire et al., 2021; Zheng et al., 2020). Wieder et al. (2015) reported a high spatial correlation (r = 0.46) of SOC (0-1 m) between MIMICS outputs and HWSD. In addition, Wang et al. (2017) observed the high consistency in SOC (0-1 m) (R^2=0.96; P<0.01) between the TRIPLEX-MICROBE model and HWSD by vegetation type. Huang et al., (2021) also found good performance of the ORCHIMIC v2.0 in reproducing SOC by comparing the simulated values with multiple SOC datasets. The

well-developed plant physiology and environmental controls in the model may explain their good performance in simulating vegetation and soil processes (Flato, 2011; Mathieu & O'Neill, 2008). However, the latitudinal trends and grid-level distribution of DOC, SOC, and MBC (sum of FBC and BBC) in the top 1 m were relatively worse reproduced than those in the top 30 cm (subfigures e-k of Figures 1 & 3, subfigures e-f of Figures 2 & 4), indicating that the vertical distribution of processes related to decomposition, microbial turnover, and plant C input needs further improvements. Although parameters classifying the active decomposition depth and biological function to perturbation were defined in the CLM-Microbe model, the gradual change of microbial turnover and activity defined along soil profile may need to be improved in future models (Preusser et al., 2019; Zhu et al., 2021). In addition, processes or parameters related to the active layer for decomposition and perturbation caused by biological (e.g., nematode) and abiotic (e.g., drying and rewetting) activities can cause uncertainties in the vertical distribution of C cycle, which needs further efforts and attention in model development (Ettema & Wardle, 2002; Gabet et al., 2003; Kuzyakov & Blagodatskaya, 2015; Schimel, 2018).

We estimated global annual averages of 129.5, 56.5, 99.8, and 49.8 PgC yr^{-1} for GPP, NPP, HR, and SR, respectively (Table 1). Consistent with our results, previous studies reported similar values of GPP, NPP, HR, and SR (Cramer et al., 1999; Hashimoto et al., 2015; Huang et al., 2020; Lu et al., 2021; Nemani et al., 2003; Zhao et al., 2017; Zheng et al., 2020). The consistent simulations and reasonable estimations of GPP, NPP, HR, and SR across models may indicate the convergent plant physiology among models, and well-defined soil and microbial processes in the CLM-Microbe model. In addition, compared with observed data, the CLM-Microbe model produced more consistent NPP and HR but overestimated GPP and SR (Table 1). The overestimation of GPP and SR may be due to the lower ecosystem-scale CUE in the CLM-Microbe model. The vegetation physiology module in the CLM-Microbe model is adapted from CLM4.5. The ecosystem-scale CUEs between the CLM-Microbe model (0.44) and CLM4.5 (0.43) were comparable but lower than in MODIS (0.5). Correspondingly, we observed a higher contribution of roots to total SR in the CLM-Microbe model (0.5) and the CLM4.5 (0.48) than in the observed SRDB dataset (0.43). Therefore, the well-simulated NPP and HR but higher predicted GPP and SR in the CLM-Microbe model were attributed to the low ecosystem-scale CUE in the CLM-Microbe. Increasing ecosystem-scale CUE in the CLM-Microbe model will improve the modeling performance of GPP and SR in model development.

The CLM-Microbe model can reasonably predict FBC, BBC, and DOC in the top 30 cm well at the global level, indicating the well-represented microbial processes in surface soils (Table 1). However, MBC and DOC in the top 1 m were vastly overestimated, with MBC and DOC in the top 1 m overestimated by 69.5% and 75.0%, respectively. Inconsistent with our results, previous studies suggested the underestimation of MBC (0-1 m) in their models. For example, Wang et al. (2017) estimated the global MBC as 21

PgC in the TRIPLEX-MICROBE model. Wieder et al. (2015) suggested the steady-state MBC (0-1 m) of 16.3 Pg in the MIMICS. The relatively poor performance of the CLM-Microbe model in simulating DOC and MBC in the top 1 m and the discrepancy in simulated MBC (0-1 m) among studies may result from three aspects. First, the hydrologically active layer in the CLM-Microbe model may not be sufficient to define soil microbial processes along soil profile. We observed better performance of the CLM-Microbe model in simulating FBC, BBC, and DOC in the top 30 cm relative to MBC and DOC in the top 1 m, indicating that the representation of microbial and soil processes along soil profile may need improvements. Second, the difference in calibration for MBC may cause discrepancy between studies. The SOC in Wieder et al. (2015) was calibrated to observed data but not MBC, Wang et al. (2017) calibrated the MBC (0-1 m) in the TRIPLEX-MICROBE by vegetation types, while we calibrated both MBC and SOC in 0-30 cm and 0-1 m by grid in the CLM-Microbe model. The differences in variables and depths calibrated between studies can partly explain the discrepancy. Third, the difference in simulated vegetation, litter, and soil C pools among studies can result in the discrepancy. Vegetation C as litter and volatile organic compounds, DOC, and SOC are the C source for microbial C assimilation through decomposition (Figure S1). Consequently, the overestimation of SOC and DOC can partly explain the overestimation of MBC in the top 1 m (Table 1).

The CLM-Microbe model indicated an underestimation of 8.5% for SOC (0-30 cm) and an overestimation of 32% for SOC (0-1 m) when comparing with observed data (Table 1). Compared with the CLM4.5, the CLM-Microbe predicted larger stocks of SOC (0-30 cm and 0-1 m). Previous studies suggest large variations in simulated SOC (0-1 m) among models. For example, Todd-Brown et al. (2013) reported the SOC (0-1 m) stock ranging from 510 to 3040 PgC among 11 CMIP5 ESMs. The TRIPLEX-MICROBE modeled the global SOC (0-1 m) stock as 1195 PgC (Wang et al., 2017). Wieder et al. (2015) documented the steady-state SOC pool in the MIMICS as 1530 PgC. Delire et al. (2020) reported the SOC (0-1 m) as 1611 PgC and 1520 PgC in the new (ISBA_bgc6) and old (ISBA_bgc5) versions, respectively, of ISBA-CTRIP. Given the wide range (510 to 3040 PgC) of simulated SOC (0-1 m) in models, the CLM-Microbe model thus predicted reasonable SOC stocks.

4.2 Temporal trends of carbon fluxes and stocks

The area-weighted average of GPP, NPP, HR, and SR in the CLM-Microbe model increased by 30, 13, 12, and 25 PgC yr^{-1}, respectively, from 1901 to 2016 (Figure 5). Consistent with our findings, Wiltshire et al. (2021) also observed the increasing trends of GPP and NPP in the JULES model, with GPP and NPP increased by about 12 and 25 PgC yr^{-1}, respectively, from 1901 to 2005. Bonan et al. (2019) observed the increase of about 20 PgC yr^{-1} of GPP, 10 PgC yr^{-1} of NPP, and 8 PgC yr^{-1} of HR from 1850 to 2014 in the CLM4.5. The global increasing rate of SR was estimated as 0.04-0.14 PgC yr^{-1} by Huang et al. (2020). Temperature, water, CO_2 concentration, and N are key factors determining plant photosynthesis, the increasing N deposition and rising CO_2

concentration and temperature may explain the enhancement of vegetation productivity under environmental change (Dusenge et al., 2019; Piñeiro et al., 2017). In this study, we observed significant and positive correlations of GPP and NPP with MAT and MAP (Figure. 14a). Although the compounding effects of such environmental change factors also have positive effects on autotrophic respiration, but to a lesser extent, leading to increasing vegetation productivity in terrestrial ecosystems (Delire et al., 2020). In addition, the rising ST (0-1 m) may explain the observed increase in HR considering the positive relationship between ST (0-1 m) and HR (Figures 14 & S2b). The increase of HR can partly explain the rising SR from 1901 to 2016 given its critical contribution to SR. In addition to HR, the increase in root respiration due to increasing C availability and rising temperature accounted for a crucial proportion of the SR increase (Bond-Lamberty & Thomson, 2010; Hashimoto et al., 2015; Piñeiro et al., 2017; Zhou et al., 2016). Therefore, the increase of GPP and NPP can be associated with environmental change (e.g., rising MAP and MAT). Increases of GPP and NPP together with rising ST and SM in top 1 m enhanced HR and SR in the last century. Similar with GPP and NPP, by 2007-2016, both LitC (0-1 m) (4 PgC) and VegC (37 PgC) increased (Figures. 6g & 6h), which is consistent with a previous study (Bonan et al., 2019). The VegC indicates the C stock of vegetation biomass, while LitC is the C loss of vegetation biomass. Increasing water availability and temperature usually have negative impacts on maintenance of vegetation biomass and litter in the soil (Delire et al., 2020), while we observed positive correlations of VegC with MAT and MAP and of LitC with SM and ST in the top 1 m (Figure. 14). Therefore, the increase of LitC (0-1 m) and VegC may attributed to increases in GPP and NPP in the last century.

The area-weighted FBC and BBC in 0-30 cm increased by 1.0 and 0.4 PgC and those in 0-1 m increased by 1.2 and 0.7 PgC, respectively, from 1901 to 2016 in the CLM-Microbe model (Figures 6a & 6d). In addition, both DOC (2.4 PgC) and SOC (34 PgC) in the top 1 m increased from 1901 to 2016 (Figures 6e & 6f). Similarly, Bonan et al. (2019) also observed the increase of SOC (0-1 m) by about 30 PgC from 1850 to 2014 in the CLM4.5. Rising temperature has negative impacts on fungal and bacterial biomass due to its facilitating effects on microbial turnover (He & Xu, 2021). Meanwhile, the observed increase in FBC and BBC in the top 30 cm and 1 m in the CLM-Microbe model, indicating the higher decomposition potential of soil microbial community (Figure S1). In addition, rising temperature and water availability promotes microbial decomposition (Allison et al., 2010; Qiu et al., 2005; Wardle & Parkinson, 1990). Despite those negative impacts on microbial biomass maintenance and SOC stabilization, we observed increases in microbial and soil C pools from 1901 to 2016. Vegetation provides the major C source for microbial C assimilation and soil C sequestration, increases in GPP and NPP can explain the increasing trends of soil and microbial C pools during 1901-2016. Litter, SOM, and DOC are three C sources for soil microbes in the CLM-Microbe model (Materials and methods; Figure S1). The positive temporal trends of DOC, LitC, and SOC can explain the increase in FBC and BBC in the CLM-Microbe model (Figure 6).

The annual averages of fluxes (GPP, NPP, HR, and SR) and pools (FBC, BBC, DOC, LitC, and SOC in the top 1 m and VegC) exhibited more rapid increases since 1980 (Figures 5 & 6). Concurrently, we observed a more rapid increase in MAT, MAP, and ST and SM in the top 1 m since 1980 (Figure S2). In line with this study, Cheng et al. (2017) analyzed SM simulations during historical (1920–2005) and future (2006–2080) periods in the CESM from CIMP5; they also found 1980 as a transition for a subsequent increase of variation during 1920-2005, indicating more rapid changes in SM after 1980. We observed significant correlations of GPP, NPP, and VegC with MAT and MAP (Figure 14a) and of HR, SR, and FBC, BBC, DOC, LitC, and SOC with ST and SM in the top 1 m (Figure 14b). Therefore, more rapid increases in MAT, MAP, and ST and SM in the top 1 m after 1980 may explain the more rapid increases of such variables since 1980.

4.3 Changes in carbon fluxes and stocks over the space and their controls

The GPP and NPP widely increased from 1901-1910 to 2007-2016 (Figures 7a & 7b, 8a-8f, and 9a & 9b). In line with this study, Zheng et al. (2020) reported that GPP in vegetated areas, particularly temperate and humid regions (e.g., most of Asia and central and southern Africa), increased from 1982 to 2017 in the revised EC-LUE model. Yue et al. (2015) observed noticeable increases in GPP and NPP in the YIBs model. The broad increase in vegetation productivity may be due to the positive effects of elevated CO_2 and N deposition (Zheng et al., 2020). In addition, temperature and water availability have a profound influence on plant growth and land C fluxes (Yue et al., 2015; Zheng et al., 2020). Our results showed significant correlations of GPP and NPP with MAT and MAP (Figures 15a-15d). The wide increase in MAP and MAT can partly explain the overall increase in GPP and NPP (Figure S3). In particular, we observed larger increases at northern high latitudes and in equatorial regions (Figures 7a & 7b, 8a-8f, 9a & 9b), resulting from large increases of GPP and NPP in eastern Asia, central and northern South America, and southern Europe. This may be related to changes in MAT and MAP, considering their significant correlations from 1901-1910 to 2007-2016 (Figures S3a & S3b). Given the significant positive correlations of GPP and NPP with MAT and MAP in southern Europe, the large relative increase of GPP and NPP may be associated with the increasing MAT and MAP in that area. However, correlations of GPP and NPP with MAT and MAP varied with latitude in Asia, correlations of GPP and NPP with MAT and MAP were significant and positive at middle and high latitudes, but negative at low latitudes. Therefore, increases in GPP and NPP at middle and high latitudes may be related to rising MAT and those at low latitudes were associated with decreasing MAP. In central and northern South America, correlations between GPP and NPP and MAT and MAP were complex. Correlations of GPP and NPP with MAT were not consistent in such areas, while GPP and NPP were consistently and positively correlated with MAP in central and northern South America. As a result, the increase of GPP and NPP in central and northern South America may be related to the increasing MAP. However, we also observed decreases in GPP and NPP in South Asia (Figures 8a-8f). The decreases in GPP

and NPP can be explained by the increases in MAT given that GPP and NPP were negatively correlated with MAT in such region (Figures S5, 15a-15d). In contrast to the increasing trend of GPP in Amazon region during 1982-2016 in this study (~+5 gC m^{-2} yr^{-2} for most grids; P<0.05), Zheng et al. (2020) observed decreased GPP in tropical regions such as the Amazon Forest from 1982 to 2017 using the revised EC-LUE model. In addition to CO_2, N deposition, and meteorology, vegetation cover and type play an important role on GPP (Zheng et al., 2020). Land use and land cover change due to management practices have substantial effects on plant growth; such effects on leaf area index were considered in the revised EC-LUE model but not in our simulation. Therefore, the discrepancy between studies may be caused by land-use effects.

The HR and SR showed a wide increase from 1901-1910 to 2007-2016 across latitudinal gradients and the globe (Figures 7c & 7d, 8k & 8l, 9c & 9d). Consistent with our findings, Huang et al. (2020) observed a globally significant increase in SR, particularly in boreal and tropical regions (e.g., northern Asia, central South America, and central and southern Africa), from 2000 to 2014. Bond-Lamberty et al. (2018) also observed an increase of HR in multiple biomes during 2000-2015. In addition, we observed similar spatial patterns of increases (e.g., higher increases at northern high latitudes and in equatorial regions) in HR and SR with those of GPP and NPP (Figures 8k & 8l, 9c & 9d). These results indicated that soil C fluxes were largely dependent on vegetation productivity which can enhance soil C fluxes due to high C allocation to belowground (Pendall et al., 2004; Prescott et al., 2020). In addition, soil C fluxes can be further increased due to facilitated decomposition in a warming world (Noh et al., 2017; Zhou et al., 2007). Temperature and water availability have a profound influence on root respiration and HR (Bond-Lamberty & Thomson, 2010; Hashimoto et al., 2015; Sinsabaugh et al., 2016). We also found significant correlations of HR and SR with ST and SM in the top 1 m (Figures 16a-16d). The increases of HR and SR can be explained by the increases in SM and ST in the top 1 m considering their significant correlations (Figures S4c & S4d). But we also observed decreases of HR and SR in the South Asia (Figures 8c & 8d). Vegetation C fixation is the major C source for ecosystems, the decreases of GPP and NPP in such regions can largely explain the decrease in HR and SR (Figures 8a-8f).

The VegC and LitC (0-1 m) also increased across latitudinal gradients, with higher increases at northern high latitudes and in equatorial regions, and the globe by 2007-2016 relative to 1901-1910 (Figures 10g & 10h, 12g-12l, and 13g-13l). The VegC and LitC are closely related to vegetation biomass production, which partly explains the similar spatial patterns of VegC and LitC (top 1 m) with those of GPP and NPP. In addition, VegC and LitC (0-1 m) are affected by environmental factors such as temperature and water availability. We found significant correlations of VegC with MAT and MAP (Figures 15e & 15f) and LitC with ST and SM in the top 1 m (Figures 16m & 16n). Similar with GPP and NPP, the increase of VegC may be associated with the increasing MAT and MAP (Figures S4a & S4b).

The DOC and SOC in the top 1 m also increased across latitude by 2007-2016 relative to 1901-1910 (Figures 10e & 10f). In addition, DOC and SOC in the top 1 m widely increased across the globe (Figures 12a-12c, 13e-13f). In line with our results, Eglin et al. (2010) also recorded increasing soil C stock in Asia and South America in response to the combined effects of atmospheric CO_2 concentration and climate simulated by ORCHIDEE–LUC from 1901 to 2002. As vegetation C input provides the major C source for SOC stabilization, the increases in GPP, NPP, VegC, and LitC (0-1 m) may partly explain the overall increase of SOC and larger increases at northern high latitudes and in equatorial regions (Figures 8a -f 8, 12g-12l, 9a & 9b, 13g & 13h). The changes in environmental conditions can also affect SOC stock. Significant correlations of SOC with ST and SM in the top 1 m were observed (Figures 16k & 16l). However, contrary to our result, Eglin et al. (2010) found a slight decrease in soil C stock in Africa from 1901 to 2002. The SOC decline in Africa may be due to the missing temporal dynamics of N deposition in the ORCHIDEE–LUC. N has important impacts on plant growth and vegetation productivity and SOC formation, especially in N-limited areas such as arid and semiarid area in most African regions (Piñeiro et al., 2017). The DOC is the balance among SOC and litter decomposition, microbial lysis, and DOC degradation (Figure S1). In addition, we observed larger increases of DOC (0-1 m) at northern high latitudes and in equatorial regions (Figures 10e). The large increase of GPP, NPP, VegC, and LitC and SOC in the top 1 m at northern high latitudes and in equatorial regions can explain the larger increase of DOC (0-1 m) in those regions (Table 1; Figures 7a & 7b, 10f-10h, 8a-8f, 12d-12l, 9a & 9b, and 13f-13h). However, we also observed decreases of DOC and SOC in the top 1 m in South Asia and central North America (Figures 12a-12f, 13e & 13f). As the primary C source is terrestrial ecosystems, decreases in vegetation C input as GPP and NPP explain their decreases in South Asia (Figures 8a-8f, 9a & 9b). Soil C is affected by environmental factors such as soil temperature and water availability. We observed negative correlations of DOC and SOC in the top 1 m with SM (0-1 m) in South Asia and with ST (0-1 m) in central North America, increases of SM (0-1 m) and ST (0-1 m) in corresponding regions by 2007-2016 relative to 1901-1910 may contribute to decreases in DOC and SOC in the top 1 m in such areas (Figures 16i-16l, S5c & S5d).

The FBC and BBC in the top 30 cm and 1 m increased across latitudes during 2007-2016 compared with 1901-1910 (Figures 10a-10d). In addition, the FBC and BBC in the top 30 cm and 1 m widely increased across the globe (Figures 11, 13a-13d). Vegetation is the major C source for soil microbes in terrestrial ecosystems, determining the total amount of C available for microbes by regulating microbial C assimilation through SOC, DOC, and litter (Schimel, 1995; Vance & Chapin, 2001; Xu et al., 2014). This spatial patterns of GPP and NPP change could explain the wide increases of FBC and BBC in the top 30 cm and 1 m in such areas, also their larger increases at high latitudes and in equatorial regions (Figure 10a -10d, 11). However, we also found slight decreases of FBC and BBC in the top 1 m in regions such as southern Australia/Oceania (Figures 11, 13a-13d). The decrease of DOC (0-1

m) may explain the widespread decrease of FBC and BBC of 30 cm and 1 m in southern Australia/Oceania (Figures 11, 13a-13d). Meanwhile, in the top 1 m, FBC and BBC were negatively correlated with ST and positively correlated to SM in southern Australia/Oceania (Figures 16e-16h). The increase of ST and SM in the top 1 m can explain the decrease of FBC and BBC in 0-30 cm and 0-1 m in southern Australia/Oceania (Figures S3c & S3d). In addition, we found decreases of FBC and BBC in the top 30 cm and 1 m in South Asia and central North America (Figures 11, 13a-13d). Since vegetation productivity is the primary C source for terrestrial ecosystems, decreases in vegetation C input as GPP and NPP explain their decreases in South Asia (Figures 8a-8f, 9a & 9b). In addition, microbial activities are affected by soil temperature and water availability. We observed negative correlations of FBC and BBC in the top 1 m with SM (0-1 m) in South Asia and with ST (0-1 m) in central North America, increases of SM (0-1 m) and ST (0-1 m) in corresponding regions from 1901-1910 to 2007-2016 may contribute to decreases in FBC and BBC in the top 30 cm and 1 m in such areas (Figures 16e-16h, S5c & S5d).

4.4 Future improvements

Although the CLM-Microbe model can well reproduce the global distribution of C in vegetation, soil, and microbes, four key improvements are identified for future work. First, soil and microbial processes along soil profiles need to be better defined. Soil and microbial variables such as DOC, SOC, FBC, and BBC in 0-30 cm were better simulated than those in 0-1 m (Table 1; Figures 1 & 3), indicating that soil and microbial processes in the deeper soil profile are not adequately modeled. Therefore, better defining soil and microbial processes with depth can help improve the model efficacy in capturing soil and microbial processes, and further reduce uncertainties in future projections of the C cycle. Second, land-use change needs to be considered in future work. In addition to changes in environmental factors, land-use change also has profound influences on the plant, soil, and microbial processes. Drastic changes in vegetation, soil, and microbial processes due to land-use change can occur at small scales, and the spatial pattern of those processes can also be changed (Pascual et al., 1997; Sampaio et al., 2007; Stevenson et al., 2016). Therefore, considering the impacts of land-use change in the CLM-Microbe model can help improve the model efficiency in capturing spatial patterns of C density and stocks in terrestrial ecosystems. The global biogeographic patterns of soil microbes and their functions have been recognized (Xu et al., 2020), this modeling study has made progress toward a full investigation of microbial patterns and mechanisms, and a community-wide microbial data system is needed to facilitate more data-model integration to improve microbial models. Lastly, factorial analysis to attribute the variations in terrestrial C fluxes will be addressed in our future work. Variations in terrestrial C fluxes and pools are driven by multiple environmental change factors that contribute individually or in combination, attributing the variations in terrestrial C fluxes and pools to environmental change factors is important for the understanding of terrestrial C fluxes and pools dynamics (Xu et al., 2010).

5 Conclusion

The ESMs incorporating microbial processes are expected to represent uncertainties in the terrestrial C cycle more comprehensively. The CLM-Microbe model can well reproduce the distribution of vegetation (GPP, NPP, LitC, and VegC), soil (HR, SR, DOC, and SOC), and microbial (FBC, BBC, and MBC) variables. In addition, fluxes (GPP and NPP) and pools (HR, SR, FBC and BBC in top 30 cm, FBC, BBC, DOC, SOC, and LitC in the top 1 m, and VegC) increased from 1901 to 2016. We widely observed increases of such variables across the globe. Slight decreases of FBC, BBC, and DOC in the top 1 m in Australia/Oceania were also observed. The increase in GPP, NPP, and VegC were significantly related to rising MAT and MAP, while increases in FBC and BBC in top 30 cm and FBC, BBC, DOC, SOC, and LitC in the top 1 m were closely associated with increasing C input from vegetation and SM and ST in the top 1 m.

This study represents one of the first attempts to simulate the spatial and temporal variations C fluxes and pool sizes of soil, vegetation, litter, and soil microbes during the last century using a microbial-explicit model – the CLM-Microbe model. As the community is moving towards a microbial-explicit Earth system model, this study provides a robust support for microbial model development and application for predicting microbial roles in the C-climate feedback. The variations in soil microbial community over historical periods and across space simulated by the CLM-Microbe model provide a crucial foundation to study the impacts of soil microbes on terrestrial biogeochemical processes.

Acknowledgments

This study has been supported by an NSF CAREER project (2145130), an NSF RAPID award (2154746), and the CSU Program for Education & Research in Biotechnology. Support for this work for M.A.M. was provided by an Early Career Award through the U.S. Department of Energy (DOE) Biological and Environmental Research Program. Oak Ridge National Laboratory is managed by UT-Battelle, LLC, under contract DE-AC05-00OR22725 with the U.S. DOE.

Author contribution

L.H. carried out model simulation, analyzed the model output, drafted the manuscript, and finalized reviewing and editing with contributions from other authors. J.R., M.M., C.L., and D.L. contributed to the experimental design and editing of the final version of the manuscript. X.X. developed the early version of the model, acquired funding, and contributed to model simulation design, result interpretation, and editing the manuscript.

Data availability statement

The sources of observational data for model validation have been clearly cited in the main text. The CLM-Microbe used in this study is available at the GitHub repository: https://github.com/email-clm/clm-microbe, and the model version used in this study has been archived (Xiaofeng Xu et al., 2022). The model outputs have been archived at the Dryad:

https://doi.org/10.5061/dryad.612jm6471. The CRUNCEP dataset version 7 is available at https://rda.ucar.edu/datasets/ds314.3/. The GPP, NPP, HR, SR, and SOC in the top 30 cm and 1 m were from CLM land-only release can be found at https://www.earthsystemgrid.org/dataset/ucar.cgd.ccsm4.CLM_LAND_ONLY.html. Any other request can be directed to the corresponding author.

Declaration of competing interest

The authors declare no competing interests.

Reference

Allison, S. D., Wallenstein, M. D., & Bradford, M. A. (2010). Soil-carbon response to warming dependent on microbial physiology. *Nature Geoscience, 3*(5), 336-340. https://www.nature.com/articles/ngeo846

Bailey, V. L., Smith, J. L., & Bolton, H. (2002). Fungal-to-bacterial ratios in soils investigated for enhanced C sequestration. *Soil Biology and Biochemistry, 34*(7), 997-1007. https://www.sciencedirect.com/science/article/pii/S0038071702000330

Boer, W. d., Folman, L. B., Summerbell, R. C., & Boddy, L. (2005). Living in a fungal world: impact of fungi on soil bacterial niche development. *FEMS Microbiology Reviews, 29*(4), 795-811. https://academic.oup.com/femsre/article/29/4/795/493265

Bonan, G. B., Lombardozzi, D. L., Wieder, W. R., Oleson, K. W., Lawrence, D. M., Hoffman, F. M., & Collier, N. (2019). Model structure and climate data uncertainty in historical simulations of the terrestrial carbon cycle (1850–2014). *Global biogeochemical cycles, 33*(10), 1310-1326. https://agupubs.onlinelibrary.wiley.com/doi/full/10.1029/2019GB006175

Bond-Lamberty, B., Bailey, V. L., Chen, M., Gough, C. M., & Vargas, R. (2018). Globally rising soil heterotrophic respiration over recent decades. *Nature, 560*(7716), 80-83. https://www.nature.com/articles/s41586-018-0358-x

Bond-Lamberty, B., & Thomson, A. (2010). Temperature-associated increases in the global soil respiration record. *Nature, 464*(7288), 579-582. https://www.nature.com/articles/nature08930/

Cheng, S., Huang, J., Ji, F., & Lin, L. (2017). Uncertainties of soil moisture in historical simulations and future projections. *Journal of Geophysical Research: Atmospheres, 122*(4), 2239-2253. https://agupubs.onlinelibrary.wiley.com/doi/full/10.1002/2016JD025871

Cramer, W., Kicklighter, D. W., Bondeau, A., Iii, B. M., Churkina, G., Nemry, B., et al. (1999). Comparing global models of terrestrial net primary productivity (NPP): overview and key results. *Global change biology, 5*(S1), 1-15. https://onlinelibrary.wiley.com/doi/abs/10.1046/j.1365-2486.1999.00009.x

https://onlinelibrary.wiley.com/doi/full/10.1046/j.1365-2486.1999.00009.x

Delire, C., Séférian, R., Decharme, B., Alkama, R., Calvet, J.-C., Carrer, D., et al. (2020). The global land carbon cycle simulated with ISBA-CTRIP: Improvements over the last decade. *Journal of Advances in Modeling Earth Systems, 12*(9), e2019MS001886. https://agupubs.onlinelibrary.wiley.com/doi/full/10.1029/2019MS001886

Demoling, F., Nilsson, L. O., & Bååth, E. (2008). Bacterial and fungal response to nitrogen fertilization in three coniferous forest soils. *Soil Biology and Biochemistry, 40*(2), 370-379. https://www.sciencedirect.com/science/article/pii/S0038071707003549

Devêvre, O. C. and Horwáth, W. R.: Decomposition of rice straw and microbial carbon use efficiency under different soil temperatures and moistures, Soil Biology and Biochemistry, 32, 1773-1785, 2000.

Dirmeyer, P. A., Gao, X., Zhao, M., Guo, Z., Oki, T., & Hanasaki, N. (2006). GSWP-2: Multimodel Analysis and Implications for Our Perception of the Land Surface. *Bulletin of the American Meteorological Society, 87*(10), 1381-1398. https://journals.ametsoc.org/view/journals/bams/87/10/bams-87-10-1381.xml

Dusenge, M. E., Duarte, A. G., & Way, D. A. (2019). Plant carbon metabolism and climate change: elevated CO_2 and temperature impacts on photosynthesis, photorespiration and respiration. *New Phytologist, 221*(1), 32-49. https://nph.onlinelibrary.wiley.com/doi/full/10.1111/nph.15283

Eglin, T., Ciais, P., Piao, S. L., Barré, P., Bellassen, V., Cadule, P., et al. (2010). Historical and future perspectives of global soil carbon response to climate and land-use changes. *Tellus B: Chemical and Physical Meteorology, 62*(5), 700-718. https://www.tandfonline.com/doi/abs/10.1111/j.1600-0889.2010.00499.x

https://www.tandfonline.com/doi/pdf/10.1111/j.1600-0889.2010.00499.x

Ettema, C. H., & Wardle, D. A. (2002). Spatial soil ecology. *Trends in ecology & evolution, 17*(4), 177-183. https://www.sciencedirect.com/science/article/pii/S0169534702024965

https://www.sciencedirect.com/science/article/pii/S0169534702024965/pdfft?md5=f393dd551648c40a3c186ad5535c025b&pid=1-s2.0-S0169534702024965-main.pdf&isDTMRedir=Y

FAO. (2018). *Global Soil Organic Carbon Map (GSOCmap) : Technical Report*. Rome, Italy: FAO.

Flato, G. M. (2011). Earth system models: an overview. *Wiley Interdisciplinary Reviews: Climate Change, 2*(6), 783-800. https://onlinelibrary.wiley.com/doi/full/10.1002/wcc.148

Gabet, E. J., Reichman, O. J., & Seabloom, E. W. (2003). The effects of bioturbation on soil processes and sediment transport. *Annual Review of Earth and Planetary Sciences, 31*(1), 249-273. https://www.annualreviews.org/doi/abs/10.1146/annurev.earth.31.100901.141314

Gomez-Casanovas, N., Matamala, R., Cook, D. R., & Gonzalez-Meler, M. A. (2012). Net ecosystem exchange modifies the relationship between the autotrophic and heterotrophic components of soil respiration with abiotic factors in prairie grasslands. *Global change biology, 18*(8), 2532-2545. https://onlinelibrary.wiley.com/doi/full/10.1111/j.1365-2486.2012.02721.x

Guo, Z., Wang, Y., Wan, Z., Zuo, Y., He, L., Li, D., et al. (2020). Soil dissolved organic carbon in terrestrial ecosystems: Global budget, spatial distribution and controls. *Global Ecology and Biogeography*. https://onlinelibrary.wiley.com/doi/full/10.1111/geb.13186

Hashimoto, S., Carvalhais, N., Ito, A., Migliavacca, M., Nishina, K., & Reichstein, M. (2015). Global spatiotemporal distribution of soil respiration modeled using a global database. *Biogeosciences, 12*(13), 4121-4132. https://bg.copernicus.org/articles/12/4121/2015/

He, L., Lai, C.-T., Mayes, M. A., Murayama, S., & Xu, X. (2021a). Microbial seasonality promotes soil respiratory carbon emission in natural ecosystems: a modeling study. *Global change biology, 27*(13), 3035-3051.

He, L., Lipson, D. A., Rodrigues, J. L. M., Mayes, M., Björk, R. G., Glaser, B., et al. (2021b). Dynamics of Fungal and Bacterial Biomass Carbon in Natural Ecosystems: Site-level Applications of the CLM-Microbe Model. *Journal of Advances in Modeling Earth Systems, 13*(2), e2020MS002283. https://agupubs.onlinelibrary.wiley.com/doi/abs/10.1029/2020MS002283

He, L., Rodrigues, J. L. M., Soudzilovskaia, N. A., Barceló, M., Olsson, P. a. A., Song, C., et al. (2020). Global biogeography of fungal and bacterial biomass carbon in topsoil. *Soil Biology and Biochemistry*, 108024. https://www.sciencedirect.com/science/article/pii/S0038071720303205

He, L., & Xu, X. (2021). Mapping soil microbial residence time at the global scale. *Global change biology, 27*(24), 6484-6497. https://onlinelibrary.wiley.com/doi/abs/10.1111/gcb.15864

Hršelová, H., Chvátalová, I., Vosátka, M., Klír, J., & Gryndler, M. (1999). Correlation of abundance of arbuscular mycorrhizal fungi, bacteria and saprophytic microfungi with soil carbon, nitrogen and phsophorus. *Folia microbiologica, 44*(6), 683-687. https://link.springer.com/article/10.1007/BF02825662

Huang, N., Wang, L., Song, X.-P., Black, T. A., Jassal, R. S., Myneni, R. B., et al. (2020). Spatial and temporal variations in global soil respiration and their relationships with climate and land cover. *Science advances, 6*(41), eabb8508. https://www.science.org/doi/full/10.1126/sciadv.abb8508

Huang, Y., Guenet, B., Wang, Y. L., and Ciais, P.: Global Simulation and Evaluation of Soil Organic Matter and Microbial Carbon and Nitrogen Stocks Using the Microbial Decomposition Model ORCHIMIC v2.0, Global Biogeochemical Cycles, 35, e2020GB006836, https://doi.org/10.1029/2020GB006836, 2021.

IPCC. (2001). Climate change 2001 : the scientific basis. *Contribution of Working Group I to the Third Assessment Report of the Intergovernmental Panel on Climate Change, 2001*. https://ci.nii.ac.jp/naid/10027437043/

IPCC. (2013). *Summary for policymakers*. Retrieved from Cambridge, United Kingdom and New York, NY, USA:

Kassambara, A., & Kassambara, M. A. (2019). Package 'ggcorrplot'. *R package version 0.1, 3*(3).

Kim, D., Lee, M.-I., & Seo, E. (2019). Improvement of soil respiration parameterization in a dynamic global vegetation model and its impact on the simulation of terrestrial carbon fluxes. *Journal of Climate, 32*(1), 127-143. https://journals.ametsoc.org/view/journals/clim/32/1/jcli-d-18-0018.1.xml

Koven, C. D., Riley, W. J., Subin, Z. M., Tang, J. Y., Torn, M. S., Collins, W. D., et al. (2013). The effect of vertically resolved soil biogeochemistry and alternate soil C and N models on C dynamics of CLM4. *Biogeosciences, 10*(11), 7109. https://bg.copernicus.org/articles/10/7109/2013/

Kuzyakov, Y., & Blagodatskaya, E. (2015). Microbial hotspots and hot moments in soil: Concept & review. *Soil Biology and Biochemistry, 83*, 184-199. https://www.sciencedirect.com/science/article/pii/S0038071715000449

https://www.sciencedirect.com/science/article/pii/S0038071715000449#bib104

Lal, R. (2004). Soil carbon sequestration to mitigate climate change. *Geoderma, 123*(1-2), 1-22. https://www.sciencedirect.com/science/article/pii/S0016706104000266

Lal, R. (2008). Promise and limitations of soils to minimize climate change. *Journal of Soil and Water Conservation, 63*(4), 113A-118A. https://www.jswconline.org/content/jswc/63/4/113A.full.pdf

Lu, H., Li, S., Ma, M., Bastrikov, V., Chen, X., Ciais, P., et al. (2021). Comparing machine learning-derived global estimates of soil respiration and its components with those from terrestrial ecosystem models. *Environmental Research Letters, 16*(5), 054048. https://iopscience.iop.org/article/10.1088/1748-9326/abf526/meta

https://iopscience.iop.org/article/10.1088/1748-9326/abf526/pdf

Manzoni, S., Schimel, J. P., & Porporato, A. (2012). Responses of soil microbial communities to water stress: results from a meta-analysis. *Ecology, 93*(4), 930-938. https://esajournals.onlinelibrary.wiley.com/doi/full/10.1890/11-0026.1

Mathieu, P.-P., & O'Neill, A. (2008). Data assimilation: From photon counts to Earth System forecasts. *Remote Sensing of Environment, 112*(4), 1258-1267. https://www.sciencedirect.com/science/article/pii/S0034425707003240

https://www.sciencedirect.com/science/article/pii/S0034425707003240/pdfft?md5=cb5db33089a276663a7611ce0e63db89&pid=1-s2.0-S0034425707003240-main.pdf&isDTMRedir=Y

Matson, P., Lohse, K. A., & Hall, S. J. (2002). The globalization of nitrogen deposition: consequences for terrestrial ecosystems. *Ambio*, 113-119. https://www.jstor.org/stable/4315223

https://www.jstor.org/stable/pdf/4315223.pdf

Meeran, K., Ingrisch, J., Reinthaler, D., Canarini, A., Müller, L., Pötsch, E. M., et al. (2021). Warming and elevated CO_2 intensify drought and recovery responses of grassland carbon allocation to soil respiration. *Global change biology, 27*(14), 3230-3243. https://doi.org/10.1111/gcb.15628. https://doi.org/10.1111/gcb.15628

Nemani, R. R., Keeling, C. D., Hashimoto, H., Jolly, W. M., Piper, S. C., Tucker, C. J., et al. (2003). Climate-driven increases in global terrestrial net primary production from 1982 to 1999. *Science, 300*(5625), 1560-1563. https://www.science.org/doi/full/10.1126/science.1082750

Noh, N. J., Kuribayashi, M., Saitoh, T. M., & Muraoka, H. (2017). Different responses of soil, heterotrophic and autotrophic respirations to a 4-year soil warming experiment in a cool-temperate deciduous broadleaved forest in central Japan. *Agricultural and Forest Meteorology, 247*, 560-570. https://www.sciencedirect.com/science/article/pii/S0168192317302976

Pascual, J. A., García, C., Hernandez, T., & Ayuso, M. (1997). Changes in the microbial activity of an arid soil amended with urban organic wastes. *Biology and Fertility of Soils, 24*(4), 429-434. https://doi.org/10.1007/s003740050268

Pendall, E., Bridgham, S., Hanson, P. J., Hungate, B., Kicklighter, D. W., Johnson, D. W., et al. (2004). Below-ground process responses to elevated CO2 and temperature: a discussion of observations, measurement methods, and models. *New Phytologist, 162*(2), 311-322. https://onlinelibrary.wiley.com/doi/abs/10.1111/j.1469-8137.2004.01053.x

https://nph.onlinelibrary.wiley.com/doi/full/10.1111/j.1469-8137.2004.01053.x

Piñeiro, J., Ochoa-Hueso, R., Delgado-Baquerizo, M., Dobrick, S., Reich, P. B., Pendall, E., & Power, S. A. (2017). Effects of elevated CO2 on fine root biomass are reduced by aridity but enhanced by soil nitrogen: A global assessment. *Scientific reports, 7*(1), 1-9. https://www.nature.com/articles/s41598-017-15728-4

Prescott, C. E., Grayston, S. J., Helmisaari, H.-S., Kaštovská, E., Körner, C., Lambers, H., et al. (2020). Surplus carbon drives allocation and plant–soil interactions. *Trends in ecology & evolution, 35*(12), 1110-1118. https://www.sciencedirect.com/science/article/pii/S0169534720302226

Preusser, S., Poll, C., Marhan, S., Angst, G., Mueller, C. W., Bachmann, J., & Kandeler, E. (2019). Fungi and bacteria respond differently to changing environmental conditions within a soil profile. *Soil Biology and Biochemistry, 137*, 107543. https://www.sciencedirect.com/science/article/pii/S003807171930207X

Qiu, S., McComb, A. J., Bell, R. W., & Davis, J. A. (2005). Response of soil microbial activity to temperature, moisture, and litter leaching on a wetland transect during seasonal refilling. *Wetlands Ecology and Management, 13*(1), 43-54.

R Core Team. (2013). R: A language and environment for statistical computing. Vienna, Austria: R Foundation for Statistical Computing. *Available*.

Sampaio, G., Nobre, C., Costa, M. H., Satyamurty, P., Soares-Filho, B. S., & Cardoso, M. (2007). Regional climate change over eastern Amazonia caused by pasture and soybean cropland expansion. *Geophysical Research Letters, 34*(17). https://agupubs.onlinelibrary.wiley.com/doi/full/10.1029/2007GL030612

Schimel, D. S. (1995). Terrestrial ecosystems and the carbon cycle. *Global change biology, 1*(1), 77-91. https://onlinelibrary.wiley.com/doi/abs/10.1111/j.1365-2486.1995.tb00008.x

Schimel, J. P. (2018). Life in dry soils: effects of drought on soil microbial communities and processes. *Annual review of ecology, evolution, and systematics, 49*, 409-432. https://www.annualreviews.org/doi/full/10.1146/annurev-ecolsys-110617-062614

Sinsabaugh, R. L., Manzoni, S., Moorhead, D. L., and Richter, A.: Carbon use efficiency of microbial communities: stoichiometry, methodology and modelling, Ecology Letters, 16, 930-939, https://doi.org/10.1111/ele.12113, 2013.

Sinsabaugh, R. L., Turner, B. L., Talbot, J. M., Waring, B. G., Powers, J. S., Kuske, C. R., et al. (2016). Stoichiometry of microbial carbon use efficiency in soils. *Ecological Monographs, 86*(2), 172-189. https://esajournals.onlinelibrary.wiley.com/doi/full/10.1890/15-2110.1

Soong, J. L., Castanha, C., Pries, C. E. H., Ofiti, N., Porras, R. C., Riley, W. J., et al. (2021). Five years of whole-soil warming led to loss of subsoil carbon stocks and increased CO_2 efflux. *Science advances, 7*(21), eabd1343. https://www.science.org/doi/abs/10.1126/sciadv.abd1343

Stevenson, B. A., Sarmah, A. K., Smernik, R., Hunter, D. W. F., & Fraser, S. (2016). Soil carbon characterization and nutrient ratios across land uses on two contrasting soils: Their relationships to microbial biomass and function. *Soil Biology and Biochemistry, 97*, 50-62. https://www.sciencedirect.com/science/article/pii/S0038071716000560

Thornton, P. E., & Rosenbloom, N. A. (2005). Ecosystem model spin-up: Estimating steady state conditions in a coupled terrestrial carbon and nitrogen cycle model. *Ecological Modelling, 189*(1-2), 25-48. https://www.sciencedirect.com/science/article/pii/S0304380005001948

Thornton, P. E., Lamarque, J.-F., Rosenbloom, N. A., and Mahowald, N. M.: Influence of carbon-nitrogen cycle coupling on land model response to CO2 fertilization and climate variability, Global Biogeochemical Cycles, 21, https://doi.org/10.1029/2006GB002868, 2007.

Todd-Brown, K. E. O., Randerson, J. T., Post, W. M., Hoffman, F. M., Tarnocai, C., Schuur, E. A. G., & Allison, S. D. (2013). Causes of variation in soil carbon simulations from CMIP5 Earth system models and comparison with observations. *Biogeosciences, 10*(3), 1717-1736. https://bg.copernicus.org/articles/10/1717/2013/

Vance, E. D., & Chapin, I. F. S. (2001). Substrate limitations to microbial activity in taiga forest floors. *Soil Biology and Biochemistry, 33*(2), 173-188. https://www.sciencedirect.com/science/article/pii/S0038071700001279

Viovy, N. (2018). *CRUNCEP Version 7 - Atmospheric Forcing Data for the Community Land Model*. Retrieved from: https://doi.org/10.5065/PZ8F-F017

Wang, G., Jagadamma, S., Mayes, M. A., Schadt, C. W., Steinweg, J. M., Gu, L., & Post, W. M. (2015). Microbial dormancy improves development and experimental validation of ecosystem model. *The ISME Journal, 9*(1), 226-237. https://www.nature.com/articles/ismej2014120

Wang, K., Peng, C., Zhu, Q., Zhou, X., Wang, M., Zhang, K., & Wang, G. (2017). Modeling global soil carbon and soil microbial carbon by integrating microbial processes into the ecosystem process model TRIPLEX-GHG. *Journal of Advances in Modeling Earth Systems, 9*(6), 2368-2384. https://agupubs.onlinelibrary.wiley.com/doi/abs/10.1002/2017MS000920

Wang, Y., Yuan, F., Arndt, K. A., Liu, J., He, L., Zuo, Y., et al. (2022). Upscaling methane flux from plot-level to eddy covariance tower domains in five Alaskan tundra ecosystems. *Frontiers in Environmental Science, 10*, 10.3389/fenvs.2022.939238.

Wang, Y., Yuan, F., Yuan, F., Gu, B., Hahn, M. S., Torn, M. S., et al. (2019). Mechanistic modeling of microtopographic impacts on CO_2 and CH_4 Fluxes in an Alaskan tundra ecosystem using the CLM-Microbe model. *Journal of Advances in Modeling Earth Systems, 11*, 17. https://agupubs.onlinelibrary.wiley.com/doi/full/10.1029/2019MS001771

Wardle, D. A., & Parkinson, D. (1990). Interactions between microclimatic variables and the soil microbial biomass. *Biology and Fertility of Soils, 9*(3), 273-280. https://doi.org/10.1007/BF00336239

Warner, D. L., Bond-Lamberty, B. P., Jian, J., Stell, E., & Vargas, R. (2019). Global Gridded 1-km Annual Soil Respiration and Uncertainty Derived from SRDB V3. In: ORNL Distributed Active Archive Center.

Wieder, W. (2014). Regridded Harmonized World Soil Database v1.2. In: ORNL Distributed Active Archive Center.

Wieder, W. R., Bonan, G. B., & Allison, S. D. (2013). Global soil carbon projections are improved by modelling microbial processes. *Nature Climate Change, 3*(10), 909-912. https://www.nature.com/articles/nclimate1951

Wieder, W. R., Grandy, A. S., Kallenbach, C. M., Taylor, P. G., & Bonan, G. B. (2015). Representing life in the Earth system with soil microbial functional traits in the MIMICS model. *Geoscientific Model Development, 8*, 1789-1808. http://adsabs.harvard.edu/abs/2015GMD.....8.1789W

Wiltshire, A. J., Burke, E. J., Chadburn, S. E., Jones, C. D., Cox, P. M., Davies-Barnard, T., et al. (2021). JULES-CN: a coupled terrestrial carbon–nitrogen scheme (JULES vn5. 1). *Geoscientific Model Development, 14*(4), 2161-2186.

Xu, X., Elias, D. A., Graham, D. E., Phelps, T. J., Carroll, S. L., Wullschleger, S. D., & Thornton, P. E. (2015). A microbial functional group-based module for simulating methane production and consumption: Application to an incubated permafrost soil. *Journal of Geophysical Research: Biogeosciences, 120*(7), 1315-1333. https://agupubs.onlinelibrary.wiley.com/doi/abs/10.1002/2015JG002935

Xu, X., He, L., & Wang, Y. (2022). CLM-Microbe v1.0. [software] *Zenodo, https://doi.org/10.5281/zenodo.7439312*.

Xu, X., Schimel, J. P., Thornton, P. E., Song, X., Yuan, F., & Goswami, S. (2014). Substrate and environmental controls on microbial assimilation of soil organic carbon: a framework for Earth system models. *Ecology Letters, 17*(5), 547-555. https://doi.org/10.1111/ele.12254

Xu, X., Thornton, P. E., & Post, W. M. (2013). A global analysis of soil microbial biomass carbon, nitrogen and phosphorus in terrestrial ecosystems. *Global Ecology and Biogeography, 22*(6), 737-749.

Xu, X., Wang, N., Lipson, D. L., Sinsabaugh, R. L., Schimel, J. P., He, L., et al. (2020). Microbial macroecology: in search of mechanisms governing microbial biogeographic patterns. *Global Ecology and Biogeography, 29*, 1870-1886.

Xu, X. F., Tian, H. Q., Zhang, C., Liu, M. L., Ren, W., Chen, G. S., et al. (2010). Attribution of spatial and temporal variations in terrestrial methane flux over North America. *Biogeosciences, 7*(11), 3637-3655.

Yue, X., Unger, N., & Zheng, Y. (2015). Distinguishing the drivers of trends in land carbon fluxes and plant volatile emissions over the past 3 decades. *Atmospheric Chemistry and Physics, 15*(20), 11931-11948. https://acp.copernicus.org/articles/15/11931/2015/

Zhang, Q., Lei, H.-M., & Yang, D.-W. (2013). Seasonal variations in soil respiration, heterotrophic respiration and autotrophic respiration of a wheat and maize rotation cropland in the North China Plain. *Agricultural and Forest Meteorology, 180*, 34-43. https://www.sciencedirect.com/science/article/pii/S0168192313001056

Zhao, M., Heinsch, F. A., Nemani, R. R., & Running, S. W. (2005). Improvements of the MODIS terrestrial gross and net primary production global data set. *Remote Sensing of Environment, 95*(2), 164-176. https://www.sciencedirect.com/science/article/pii/S0034425705000106

Zhao, Z., Peng, C., Yang, Q., Meng, F.-R., Song, X., Chen, S., et al. (2017). Model prediction of biome-specific global soil respiration from 1960 to 2012. *Earth's Future, 5*(7), 715-729. https://onlinelibrary.wiley.com/doi/abs/10.1002/2016EF000480

Zheng, Y., Shen, R., Wang, Y., Li, X., Liu, S., Liang, S., et al. (2020). Improved estimate of global gross primary production for reproducing its long-term variation, 1982–2017. *Earth System Science Data, 12*(4), 2725-2746.

Zhou, L., Zhou, X., Shao, J., Nie, Y., He, Y., Jiang, L., et al. (2016). Interactive effects of global change factors on soil respiration and its components: a meta-analysis. *Global Change Biology, 22*(9), 3157-3169. https://onlinelibrary.wiley.com/doi/full/10.1111/gcb.13253

Zhou, X., Wan, S., & Luo, Y. (2007). Source components and interannual variability of soil CO_2 efflux under experimental warming and clipping in a grassland ecosystem. *Global Change Biology, 13*(4), 761-775. https://onlinelibrary.wiley.com/doi/full/10.1111/j.1365-2486.2007.01333.x

Zhu, X., Zhang, L., Zuo, Y., Liu, J., Yu, J., Yuan, F., et al. (2021). Wetland reclamation homogenizes microbial properties along soil profiles. *Geoderma, 395*, 115075. https://www.sciencedirect.com/science/article/pii/S001670612100149X

Table 1. Annual flux of GPP, NPP, HR, and SR and carbon stocks of FBC in the top 30 cm, BBC in the top 30 cm, MBC (0-1 m), DOC in the top 30 cm, SOC in the top 30 cm, and SOC in the top 1 m by observed datasets and by simulations of the CLM-Microbe model and CLM4.5 at the global scale

		Global estimation		
Variables	Unit	Observed	CLM-Microbe	CLM4.5
GPP	PgC yr^{-1}	111.94	129.53	120.13
NPP		55.76	56.49	51.26
SR		86.34	99.80	89.79
HR		49.01	49.84	46.87
FBC (0-30 cm)	PgC	13.57	13.12	--
BBC (0-30 cm)		3.29	4.17	--
MBC (0-1 m)		23.70	40.18	--
DOC (0-30 cm)		7.16	8.94	--
DOC (0-1 m)		12.90	22.57	--
SOC (0-30 cm)		661.71	605.27	513.40
SOC (0-1 m)		1231.99	1630.90	967.87

GPP: gross primary productivity; NPP: net primary productivity; HR: heterotrophic respiration; SR: soil respiration; DOC: dissolved organic carbon; SOC: soil organic carbon; FBC: fungal biomass carbon; BBC: bacterial biomass carbon; MBC: microbial biomass carbon. -- denoted not available. The SOC (0-1 m) data were from the Harmonized World Soil Database (HWSD, https://daac.ornl.gov/cgi-bin/dsviewer.pl?ds_id=1247); the SOC (0-30 cm) data were from the Global Soil Organic Carbon Map (GSOCmap) version 1.5; GPP and NPP data were from MODIS gridded datasets (http://files.ntsg.umt.edu/data/NTSG_Products/); the SR and HR data were from Global Gridded 1-km Annual Soil Respiration Database (SRDB) version 3 (https://daac.ornl.gov/CMS/guides/CMS_Global_Soil_Respiration.html); the FBC and BBC in the top 30 cm were from He et al. (2020); MBC (0-1 m) was compared with Xiaofeng Xu et al. (2013); the DOC (0-30 cm and 0-1 m) was derived from Guo et al. (2020). Output of the CLM-Microbe model during 2000-2009 (decadal average) were used to compare with observational data.

Table 2. Carbon stock of vegetation, litter, and soil pools and absolute and relative changes from 1901-1910 to 2007-2016

	Total Carbon stock (PgC)		Change from 1901-1910 to 2007-2016	
Pool	1901-1910	2007-2016	Absolute change (PgC)	Relative change (%)
SOC	4527 (0.4)	4564 (1.8)	37.0*	0.8
Litter	63 (0.2)	68 (0.4)	5.1*	8.0
Vegetation	193 (1.1)	230 (2.9)	37.1*	19.2

975 Numbers in parentheses represent standard deviation. * indicates significant absolute change from 1901-1910 to 2007-2016 at $\alpha = 0.05$.

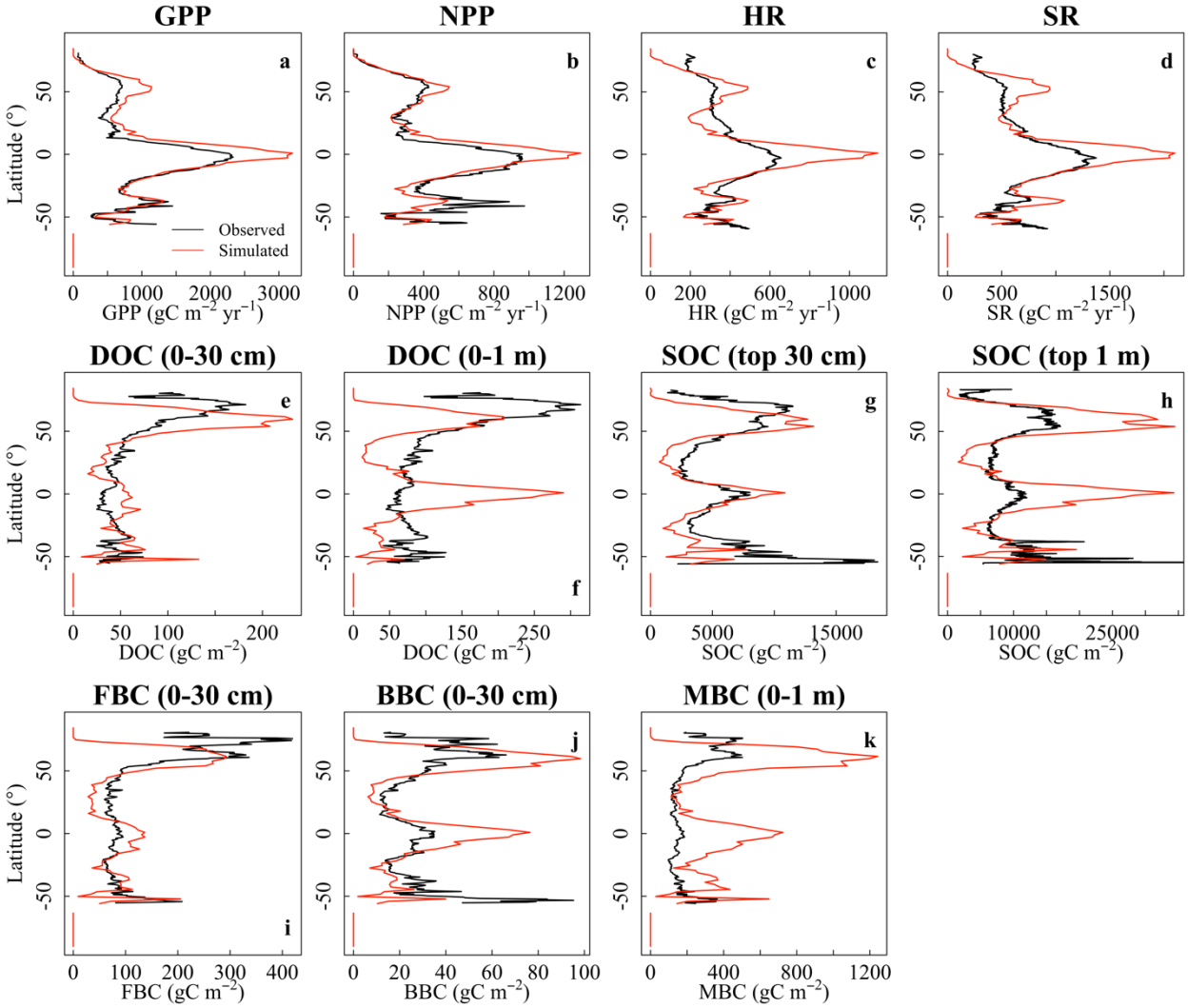

Fig. 1. Latitudinal comparison between observed (black line) and the CLM-Microbe-simulated (red line) (a) GPP, (b) NPP, (c) HR, (d) SR, (e) DOC in the top 30 cm, (f) DOC in the top 1 m, (g) SOC in the top 30 cm, (h) SOC in the top 1 m, (i) FBC in the top 30 cm, (j) BBC in the top 30 cm, and (k) MBC (0-1 m). GPP: gross primary productivity; NPP: net primary productivity; HR: heterotrophic respiration; SR: soil respiration; DOC: dissolved organic carbon; SOC: soil organic carbon; FBC: fungal biomass carbon; BBC: bacterial biomass carbon; MBC: microbial biomass carbon.

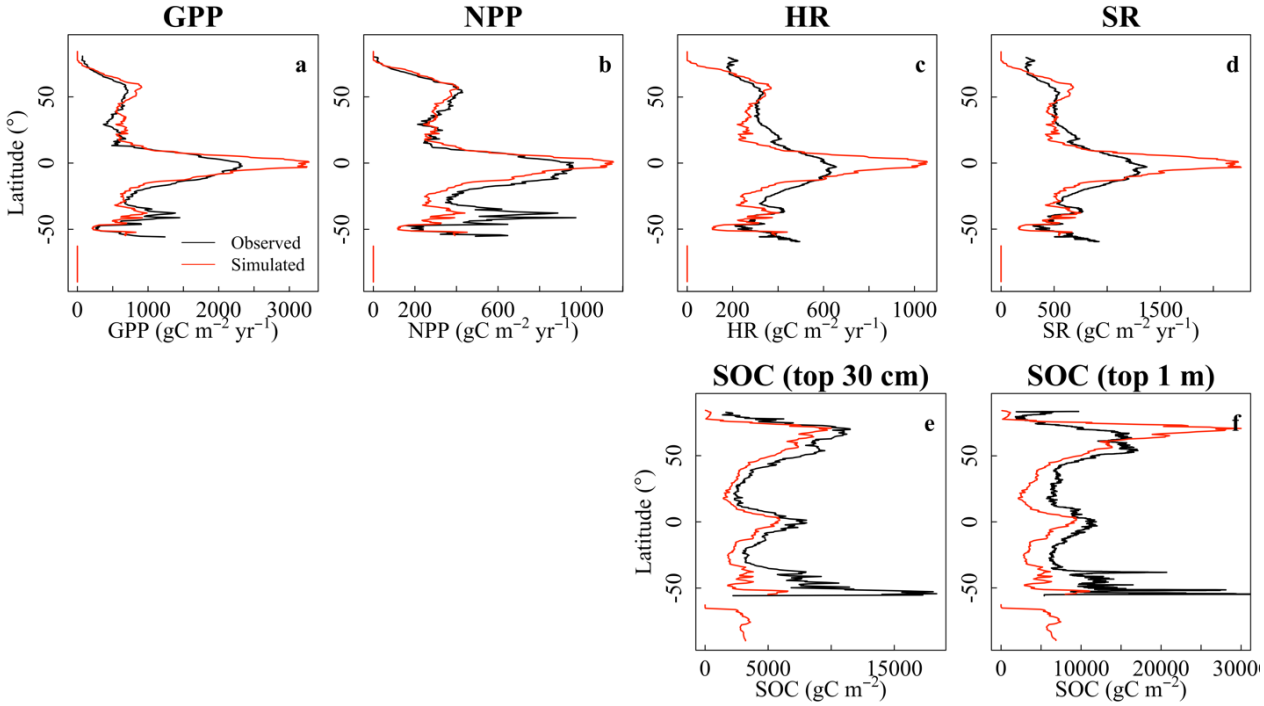

985

Fig. 2. Latitudinal comparison between observed (black line) and the CLM4.5-simulated (red line) latitudinal gradients of (a) GPP, (b) NPP, (c) HR, (d) SR, (e) SOC in the top 30 cm, and (f) SOC in the top 1 m. GPP: gross primary productivity; NPP: net primary productivity; HR: heterotrophic respiration; SR: soil respiration; SOC: soil organic carbon.

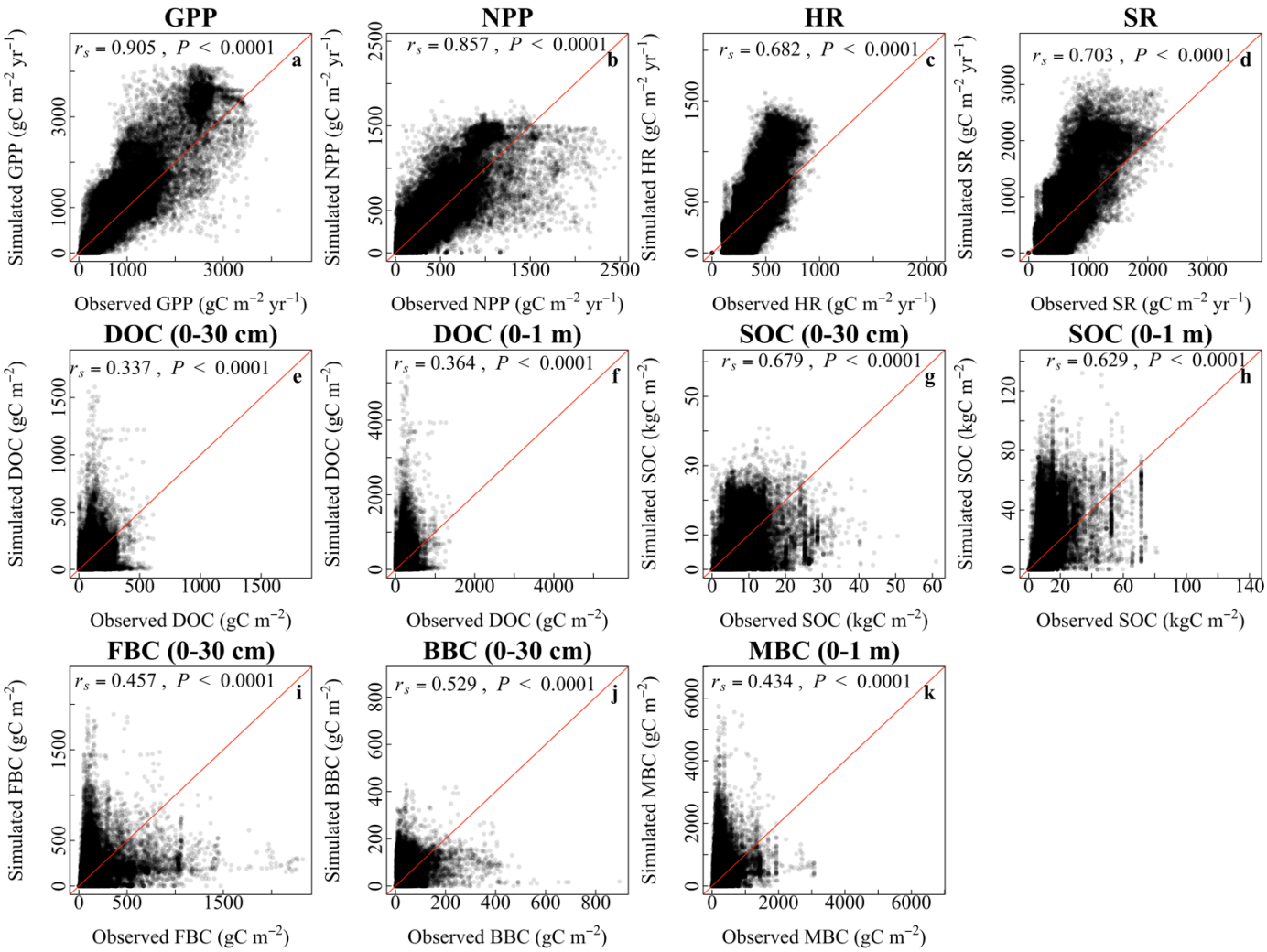

990 **Fig. 3.** Grid-by-grid comparison between observed and the CLM-Microbe-simulated (a) GPP, (b) NPP, (c) HR, (d) SR, (e) DOC in the top 30 cm, (f) DOC in the top 1 m, (g) SOC in the top 30 cm, (h) SOC in the top 1 m, (i) FBC in the top 30 cm, (j) BBC in the top 30 cm, and (k) MBC (0-1 m). Red lines are 1:1 line. GPP: gross primary productivity; NPP: net primary productivity; HR: heterotrophic respiration; SR: soil respiration; DOC: dissolved organic carbon; SOC: soil organic carbon; FBC: fungal
995 biomass carbon; BBC: bacterial biomass carbon; MBC: microbial biomass carbon.

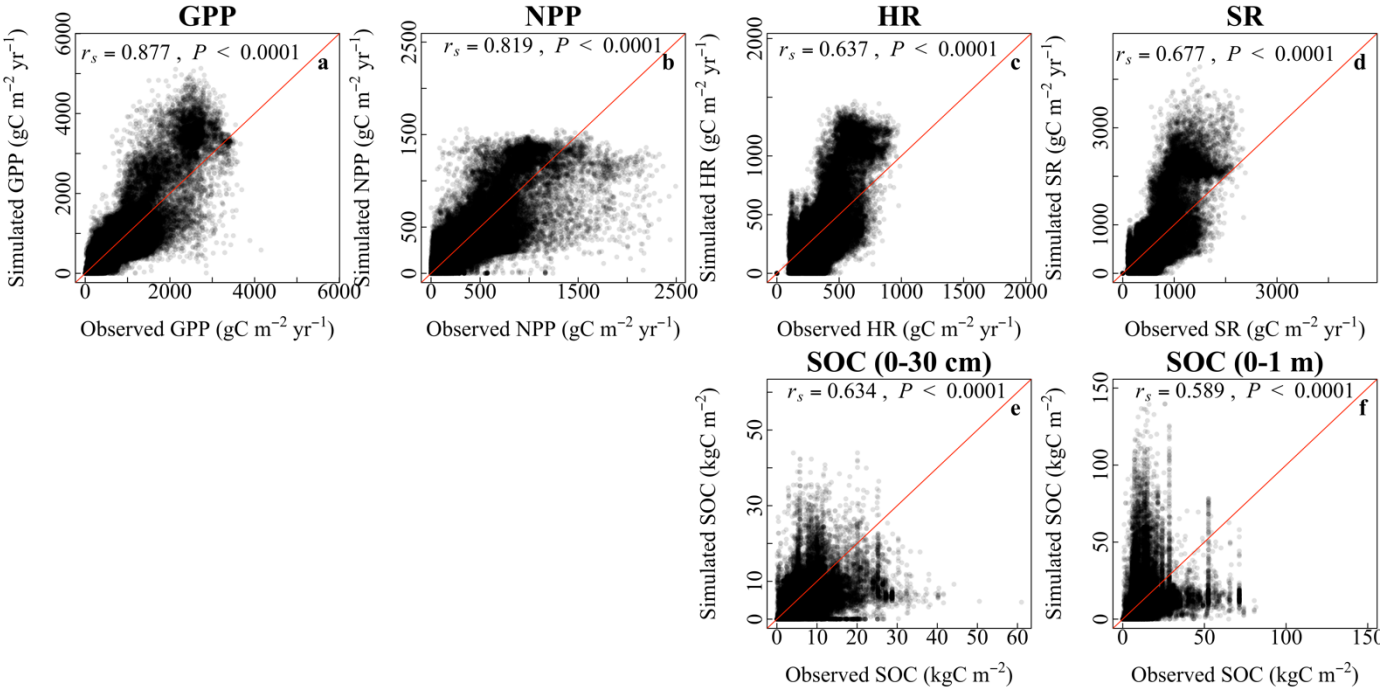

Fig. 4. Grid-by-grid comparison between observed and the CLM4.5-simulated grid cells of (a) GPP, (b) NPP, (c) HR, (d) SR, € SOC in the top 30 cm, and (f) SOC in the top 1 m. Red lines are 1:1 line. GPP: gross primary productivity; NPP: net primary productivity; HR: heterotrophic respiration; SR: soil respiration; SOC: soil organic carbon.

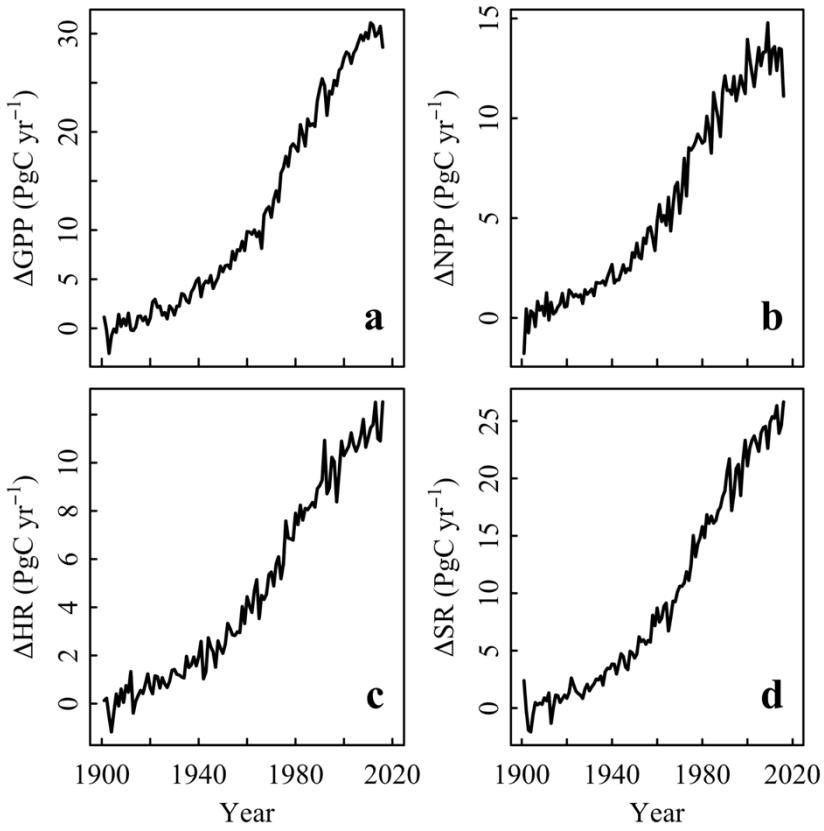

Fig. 5. Evolution of annual carbon flux of area-weighted (a) GPP, (b) NPP, (c) HR, and (d) SR simulated by the CLM-Microbe model since 1901. The baseline was the ten-year average of corresponding variables during 1901-1910. GPP: gross primary productivity; NPP: net primary productivity; HR: heterotrophic respiration; SR: soil respiration.

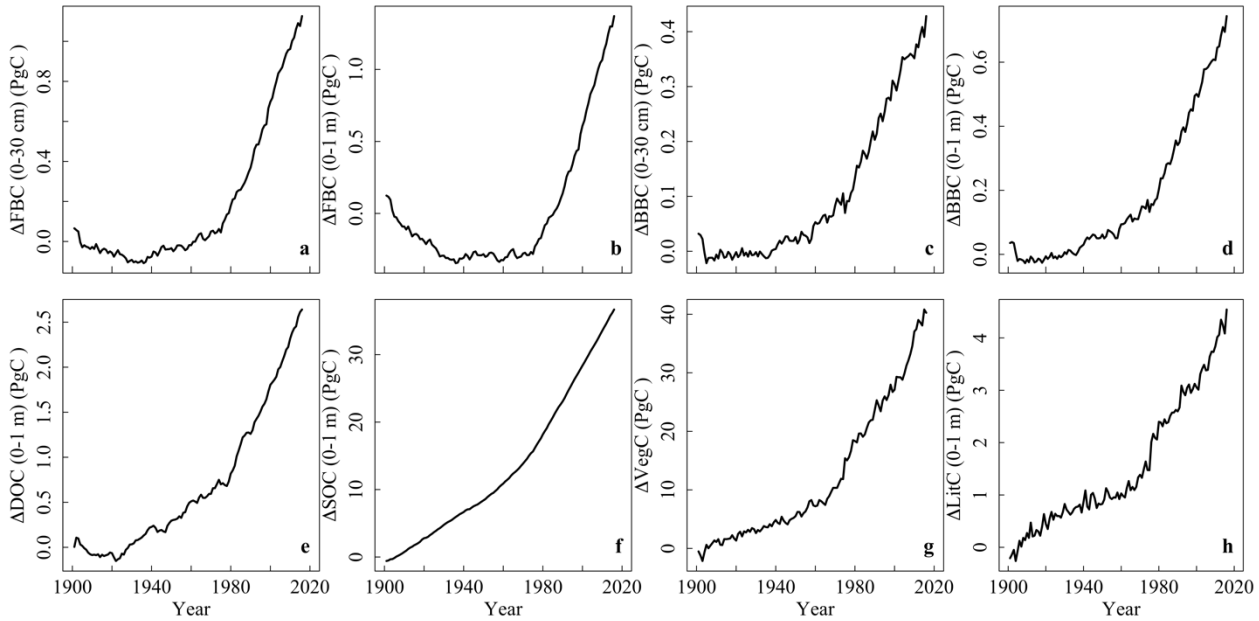

Fig. 6. Evolution of global carbon stocks of area-weighted (a) FBC in the top 30 cm, (b) FBC in the top 1 m, (c) BBC in the top 30 cm, (d) BBC in the top 1 m, (e) DOC in the top 1 m, (f) SOC in the top 1 m, and (g) VegC, and (h) LitC in the top 1 m simulated by the CLM-Microbe model since 1901. The baseline was the ten-year average of corresponding variables during 1901-1910. DOC: dissolved organic carbon; SOC: soil organic carbon; FBC: fungal biomass carbon; BBC: bacterial biomass carbon; MBC: microbial biomass carbon; VegC: vegetation carbon; LitC: litter carbon.

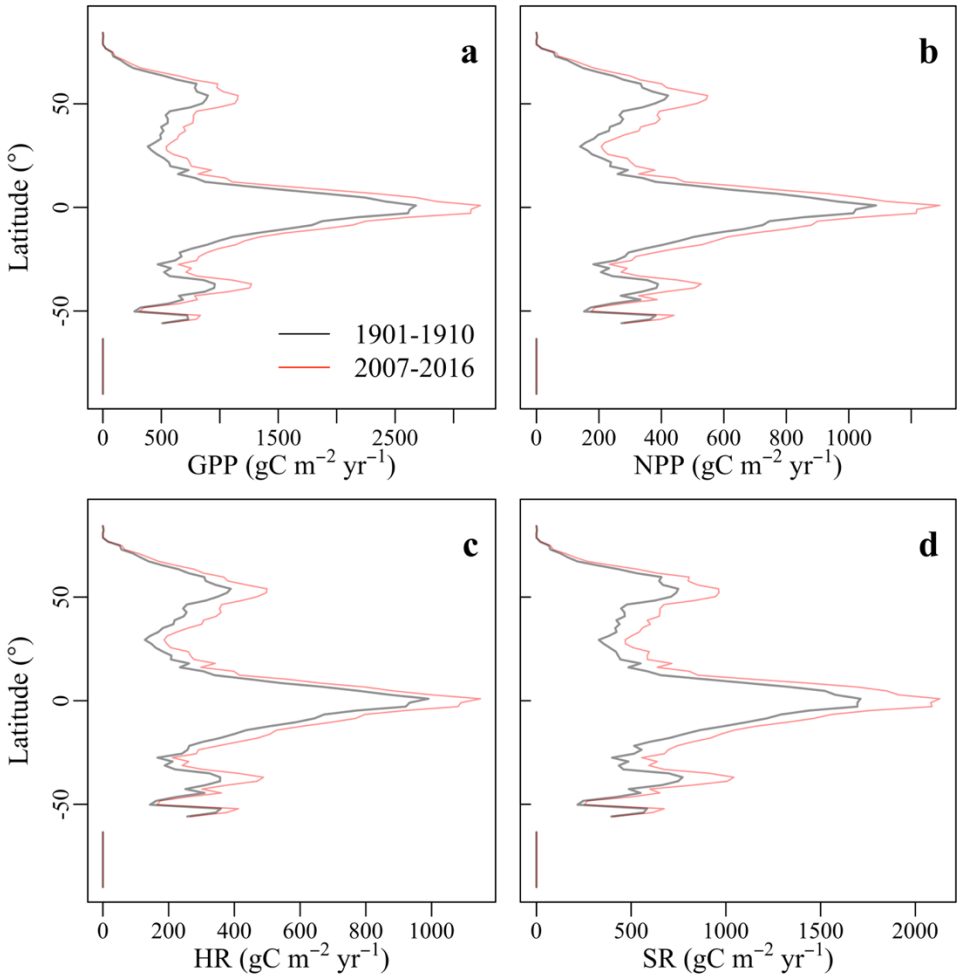

Fig. 7. Latitudinal gradients of the CLM-Microbe model simulated ten-year averages of (a) GPP, (b) NPP, (c) HR, and (d) SR during 1901-1910 and 2007-2016. GPP: gross primary productivity; NPP: net primary productivity; HR: heterotrophic respiration; SR: soil respiration.

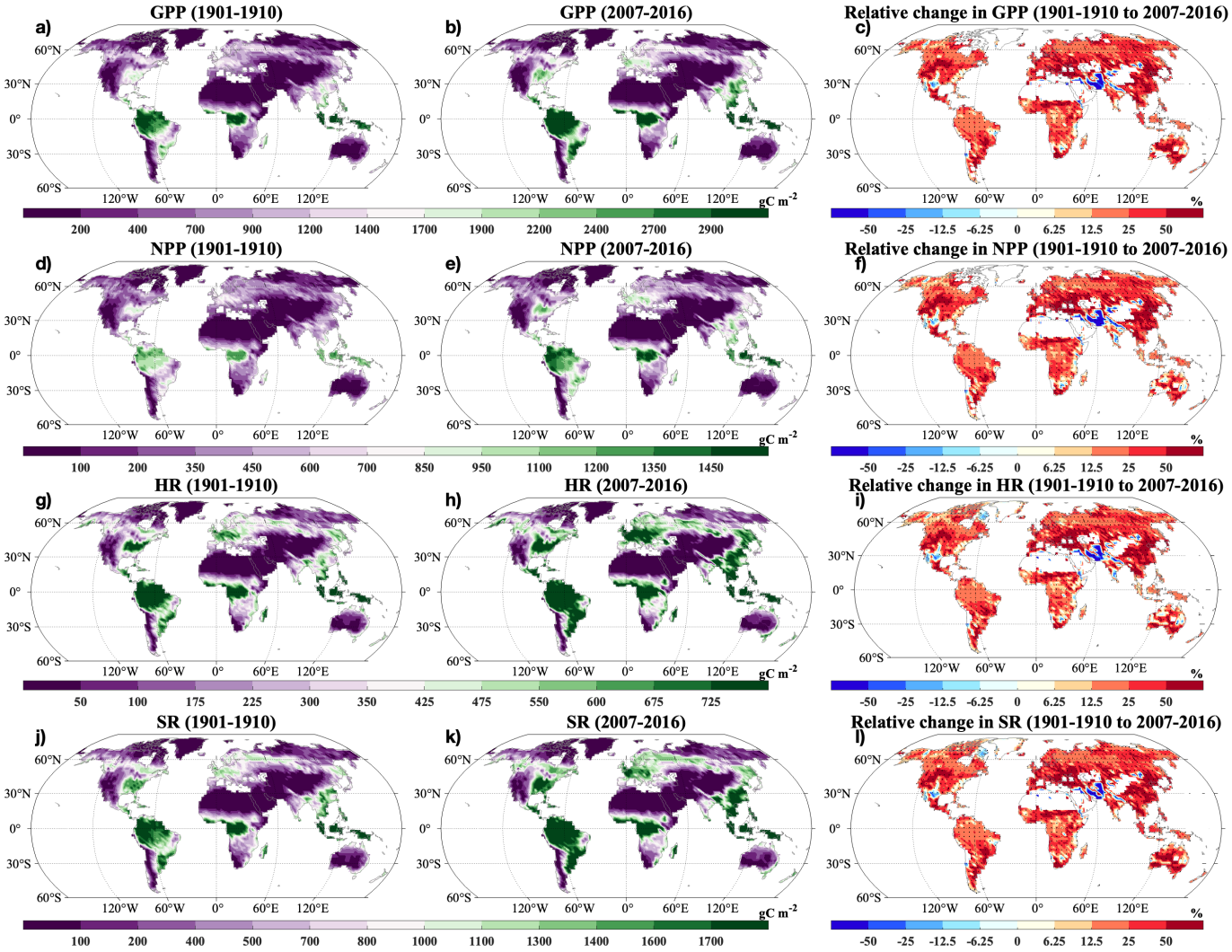

Fig. 8. Spatial distributions of decadal averages of (a-b) GPP, (d-e) NPP, (g-h) HR, and (j-k) SR during (a, d, g, and j) 1901-1910 and (b, e, h, and k) 2007-2016 and relative changes in (c) GPP, (f) NPP, (i) HR, and (l) SR by 2007-2016 relative to 1901-1910. GPP: gross primary productivity; NPP: net primary productivity; HR: heterotrophic respiration; SR: soil respiration.

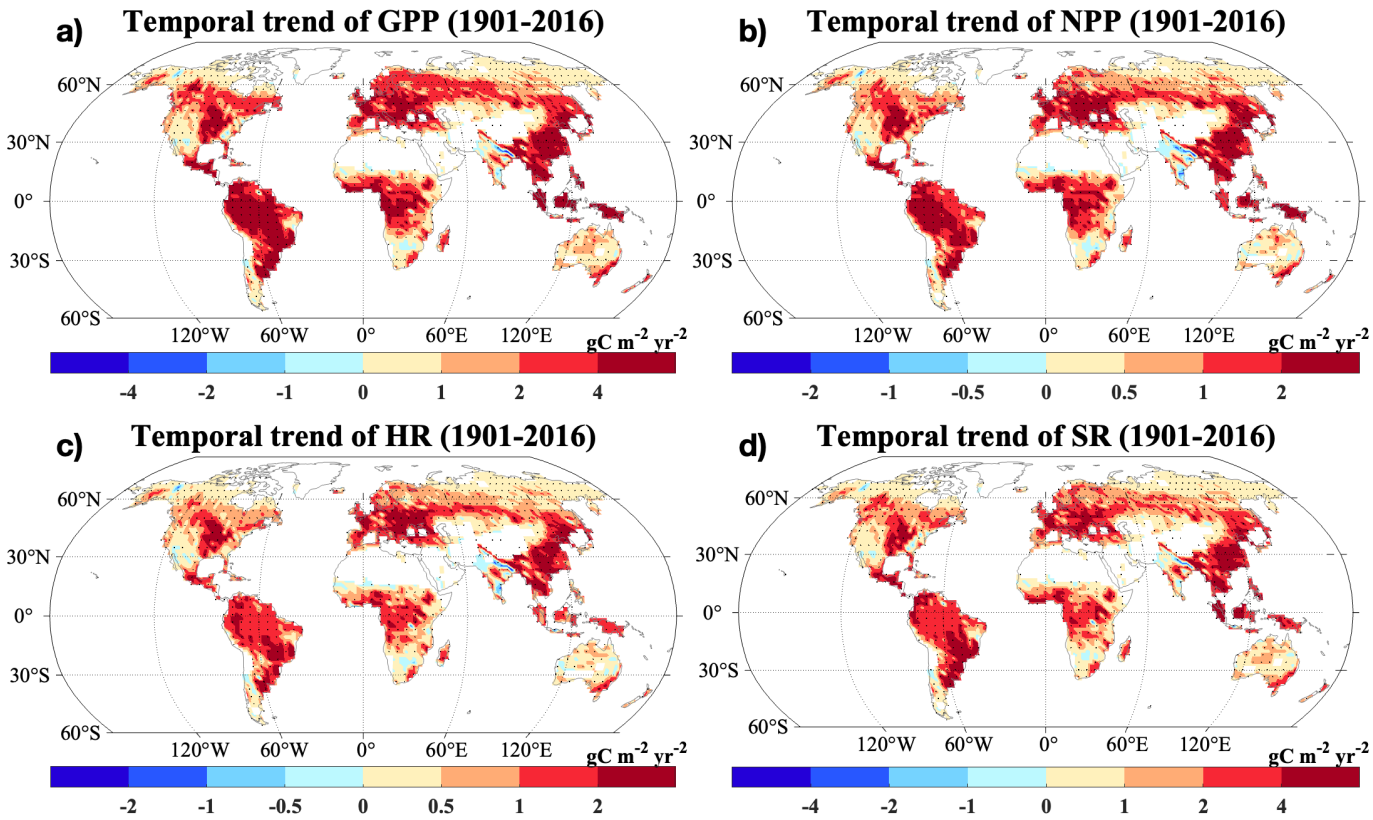

Fig. 9. Changing rates of the CLM-Microbe model simulated (a) GPP, (b) NPP, (c) HR, and (d) SR from 1901 to 2016. GPP: gross primary productivity; NPP: net primary productivity; HR: heterotrophic respiration; SR: soil respiration. Black dot in each grid indicates significant regression (P<0.05).

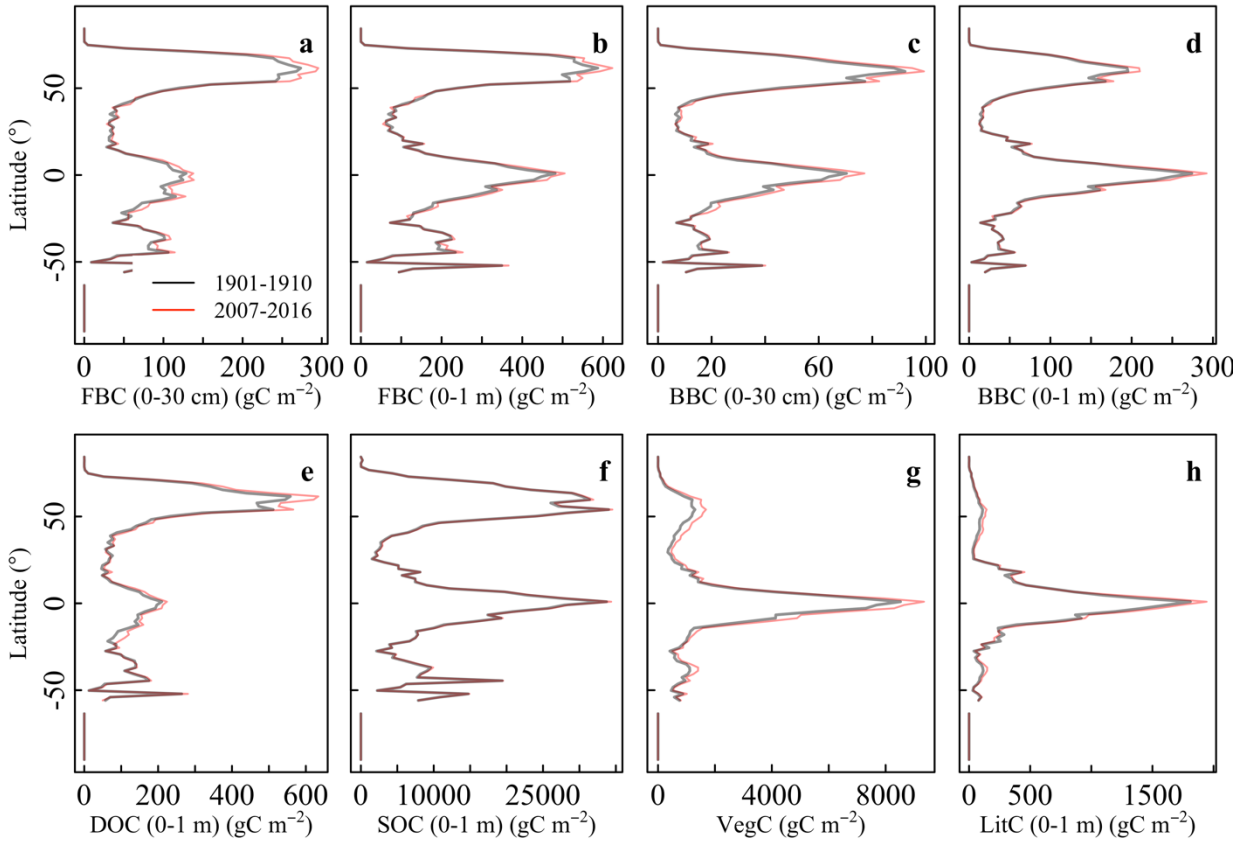

Fig. 10. Latitudinal gradients of the CLM-Microbe model simulated ten-year averages (a) FBC in the top 30 cm, (b) FBC in the top 1 m, (c) BBC in the top 30 cm, (d) BBC in the top 1 m, (e) DOC in the top 1 m, (f) SOC in the top 1 m, and (g) VegC, and (h) LitC in the top 1 m during 1901-1910 and 2007-2016. FBC: fungal biomass carbon; BBC: bacterial biomass carbon; DOC: dissolved organic carbon; SOC: soil organic carbon; VegC: vegetation carbon; LitC: litter carbon.

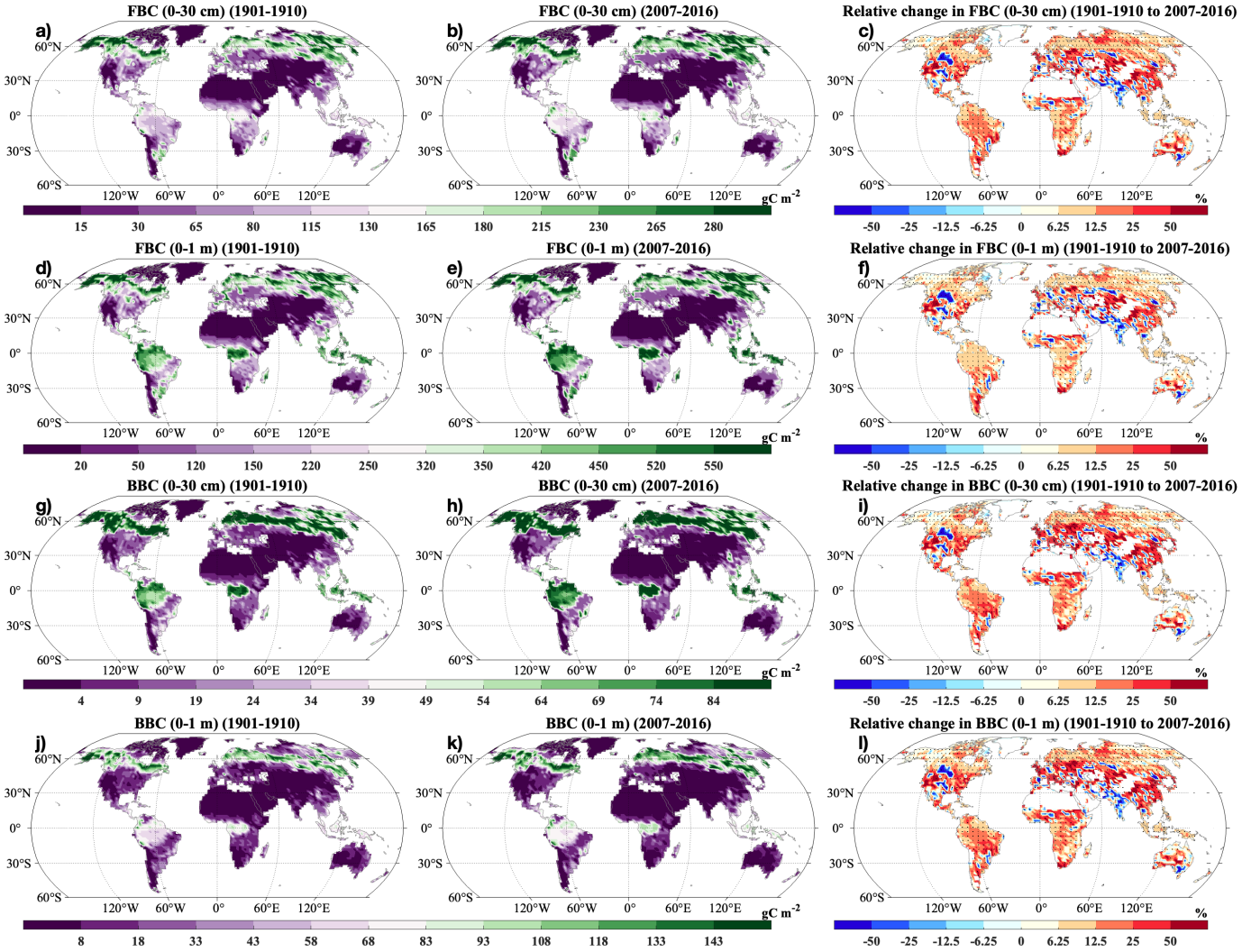

Fig. 11. Spatial distributions of decadal averages of (a-b) FBC in the top 30 cm, (d-e) FBC in the top 1 m, (g-h) BBC in the top 30 cm, and (j-k) BBC in the top 1 m during (a, d, g, and j) 1901-1910 and (b, e, h, and k) 2007-2016 and relative changes in (c) GPP, (f) NPP, (i) HR, and (l) SR by 2007-2016 relative to 1901-1910. FBC: fungal biomass carbon; BBC: bacterial biomass carbon.

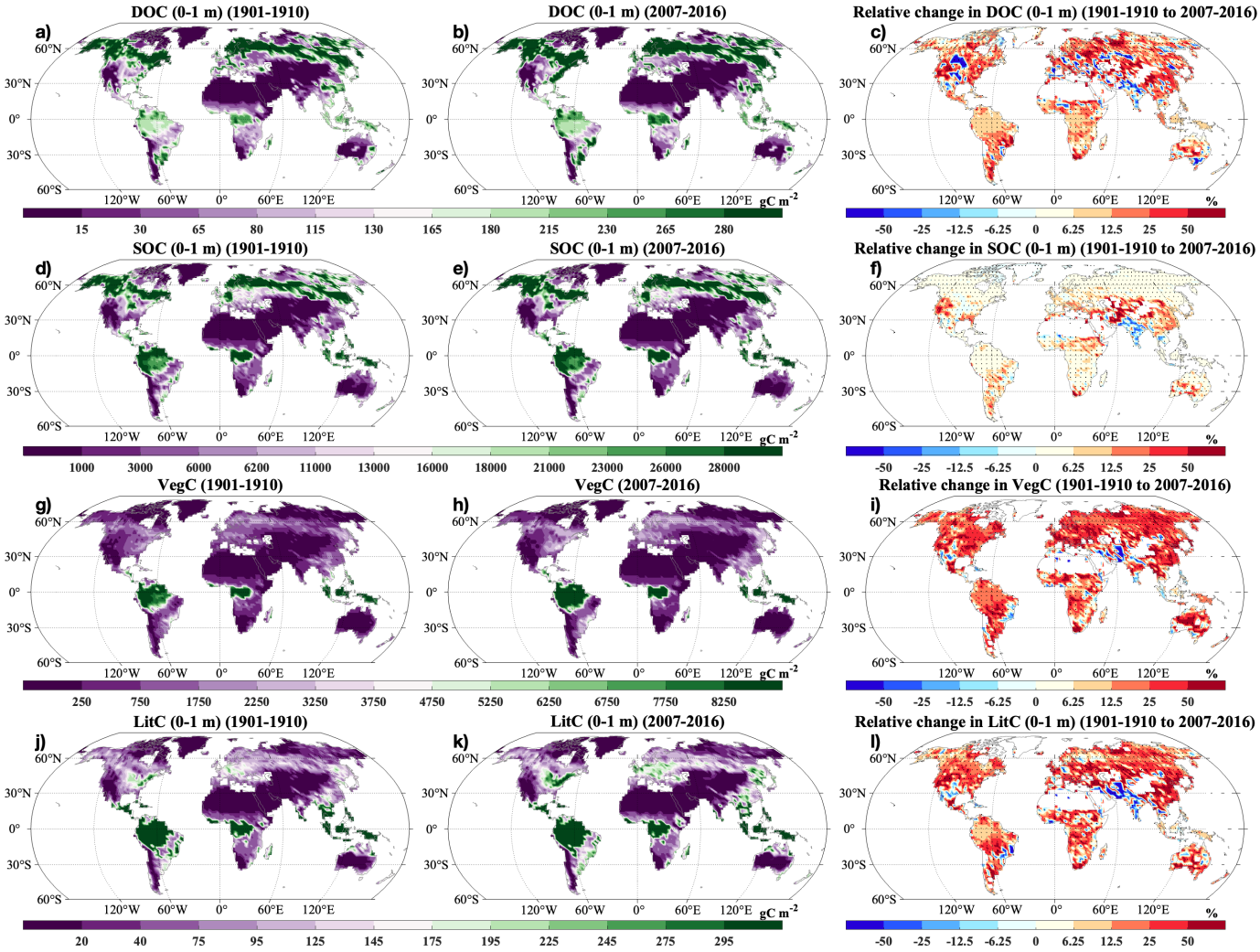

Fig. 12. Spatial distributions of decadal averages of (a-b) DOC in the top 1 m, (d-e) SOC in the top 1 m, (g-h) VegC, and (j-k) LitC in the top 1 m during (a, d, g, and j) 1901-1910 and (b, e, h, and k) 2007-2016 and relative changes in (c) DOC in the top 1 m, (f) SOC in the top 1 m, (i) VegC, and (l) LitC in the top 1 m by 2007-2016 relative to 1901-1910. DOC: dissolved organic carbon; SOC: soil organic carbon; VegC: vegetation carbon; LitC: litter carbon.

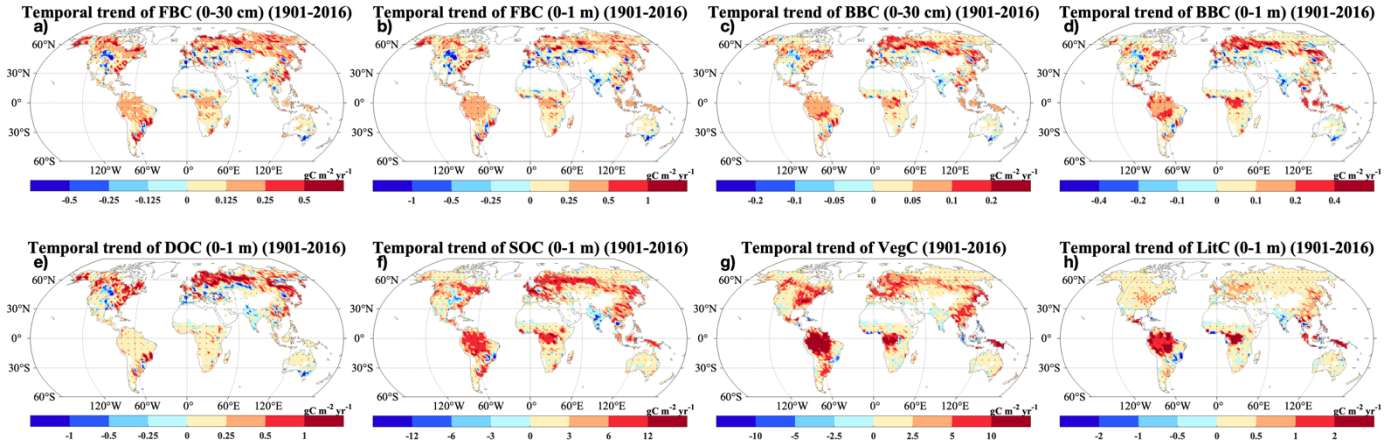

Fig. 13. Changing rates of the CLM-Microbe model simulated (a) FBC in the top 30 cm, (b) FBC in the top 1 m, (c) BBC in the top 30 cm, (d) BBC in the top 1 m, (e) DOC in the top 1 m, (f) SOC in the top 1 m, and (g) VegC, and (h) LitC in the top 1 m from 1901 to 2016. FBC: fungal biomass carbon; BBC: bacterial biomass carbon; DOC: dissolved organic carbon; SOC: soil organic carbon; VegC: vegetation carbon; LitC: litter carbon. Black dot in each grid indicates significant regression (P<0.05).

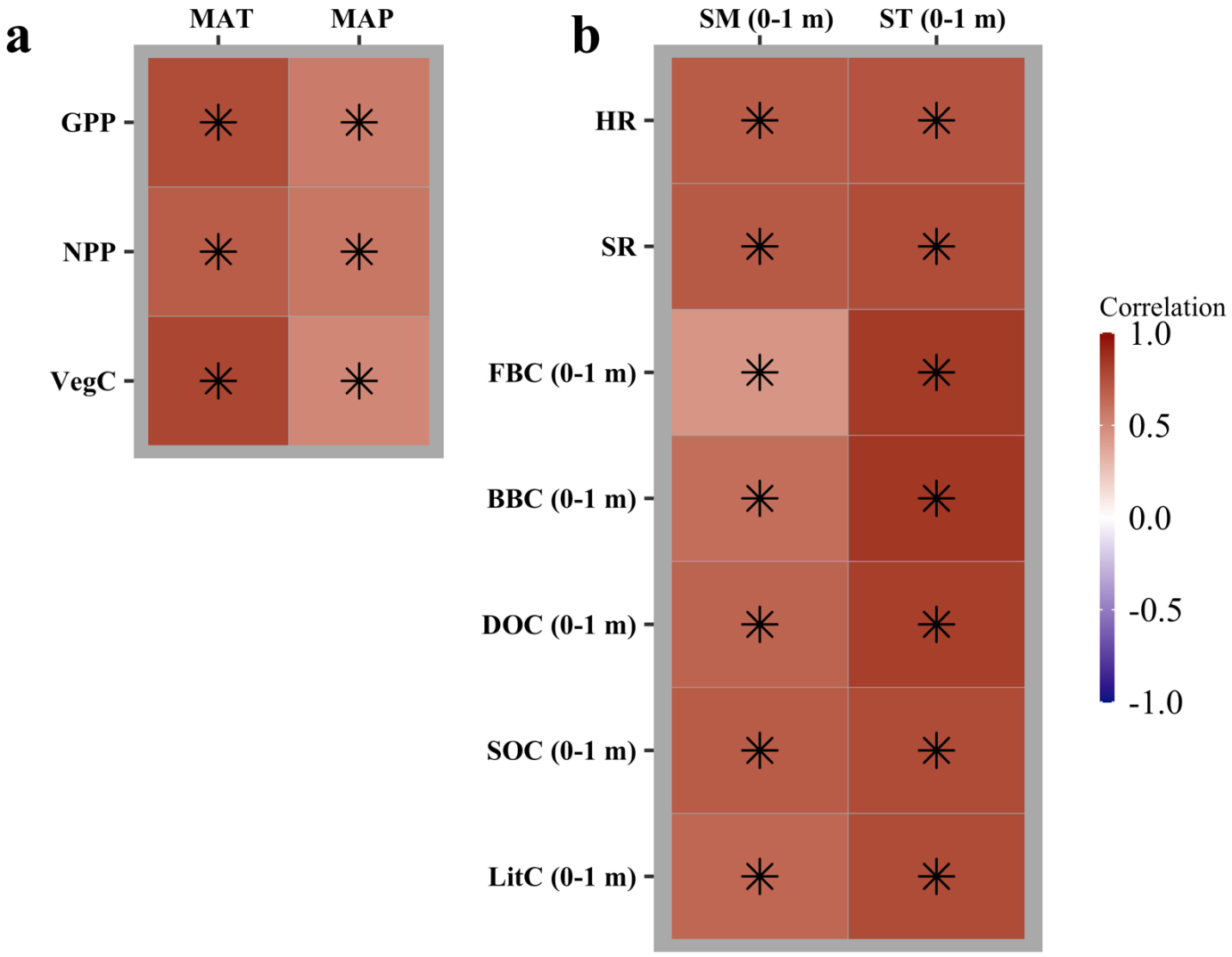

Fig. 14. Heatmap showing Pearson's correlation between the CLM-Microbe model simulated (a) GPP, NPP, and VegC and MAT and MAP and (b) HR, SR, FBC in the top 1 m, BBC in the top 1 1 m, DOC in the top 1 m, SOC in the top 1 m, and LitC in the top 1 m and SM and ST in the top 1 m from 1901 to 2016. GPP: gross primary productivity; NPP: net primary productivity; HR: heterotrophic respiration; SR: soil respiration; DOC: dissolved organic carbon; SOC: soil organic carbon; FBC: fungal biomass carbon; BBC: bacterial biomass carbon; VegC: vegetation carbon; LitC: litter carbon; MAT: mean annual temperature; MAP: mean annual precipitation; ST: soil temperature; SM: soil moisture. Black asterisks indicate significant correlations (P<0.05).

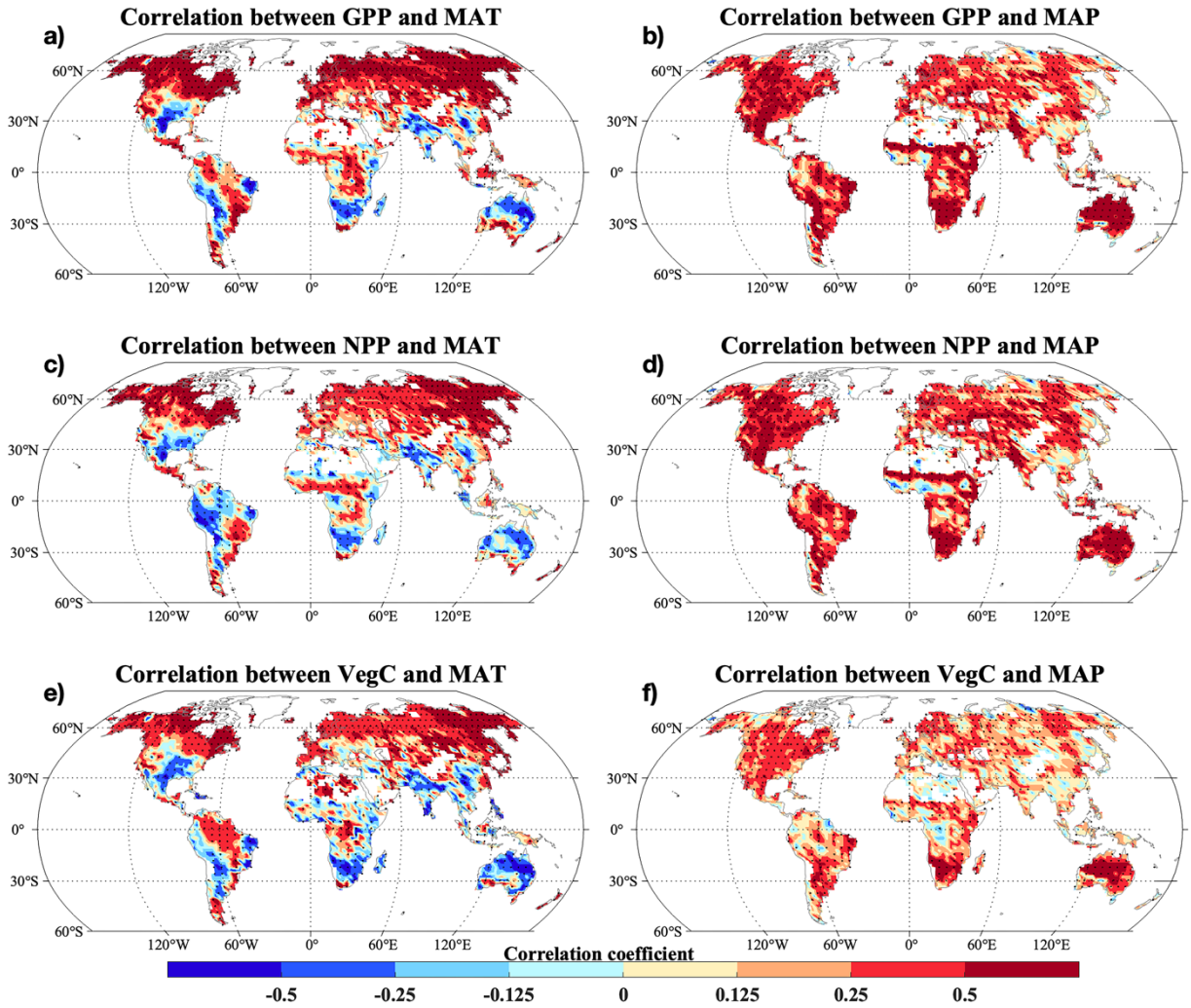

Fig. 15. Pearson's correlation between the CLM-Microbe model simulated (a-b) GPP, (c-d) NPP, and (e-f) VegC and (a, c, and e) MAT and (b, d, and f) MAP from 1901 to 2016. GPP: gross primary productivity; NPP: net primary productivity; VegC: vegetation carbon; MAT: mean annual temperature; MAP: mean annual precipitation. Black dot in each grid indicates significant correlation (P<0.05).

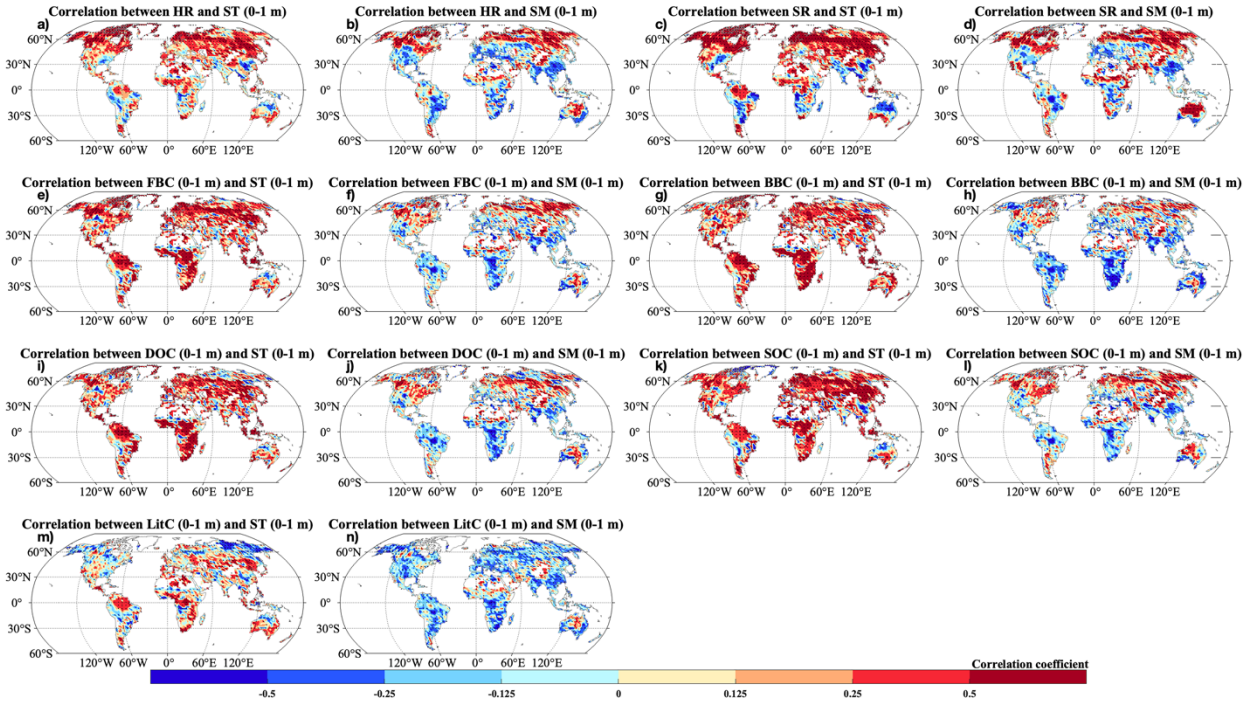

Fig. 16. Pearson's correlation between the CLM-Microbe model simulated (a-b) HR, (c-d) SR, (e-f) FBC in the top 1 m, (g-h) BBC in the top 1 m, (i-j) DOC in the top 1 m, (k-l) SOC in the top 1 m, and (m-n) LitC and (a, c, e, g, i, k, and m) ST and (b, d, f, h, j, l, and n) SM in the top 1 m from 1901 to 2016. HR: heterotrophic respiration; SR: soil respiration; FBC: fungal biomass carbon; BBC: bacterial biomass carbon; DOC: dissolved organic carbon; SOC: soil organic carbon; LitC: litter carbon; ST: soil temperature; SM: soil moisture. Black dot in each grid indicates significant correlation (P<0.05)